COMPUTATIONAL STUDY OF DIFFERENTIAL CAPACITANCE-DOUBLE

LAYER RELATIONSHIP IN A SUPERCAPACITOR

By

PRANAV MILIND PHADTARE

Presented to the Faculty of the Graduate School of

The University of Texas at Arlington in Partial Fulfillment

Of the Requirements

For the Degree of

MASTER OF SCIENCE IN MECHANICAL ENGINEERING

THE UNIVERSITY OF TEXAS AT ARLINGTON

May 2016

Acknowledgements

I would like to thank my supervising professor, Dr. Bo Yang for his guidance, patience and support during the course of this research work. His invaluable advice and encouragement enabled me to complete my thesis in timely manner. The opportunity provided to me was a great learning experience. I would also like to thank Dr. Kent Lawrence and Dr. Donghyun Shin for serving on my thesis committee.

I would also like to thank Ms. Debi Barton and Ms. Flora Pinegar for helping me in educational matters. They have always supported for the last two years at the university. I am obliged to Dr. Seiichi Nomura for his help.

I extend my thanks to all my friends at Meadow 265 and my roommates at GC 208 for the emotional support. Lastly, I am grateful to my family for supporting me emotionally and financially. I would not have completed my degree without their support and good wishes.

April 21, 2016

Abstract

COMPUTATIONAL STUDY OF DIFFERENTIAL CAPACITANCE-DOUBLE

LAYER RELATIONSHIP IN A SUPERCAPACITOR

Pranav Phadtare, MS

The University of Texas at Arlington, 2016

Supervising Professor: Bo Yang

Energy crisis is one of the most pressing problems that the world is facing. It involves a number of issues to be addressed in energy sources, transportation, storage, etc. Novel ways of energy storage are being actively explored. Electrical energy is stored by using devices such as batteries, capacitors, supercapacitors, etc. Supercapacitor seems to be a promising technology for this purpose. Traditionally, batteries have high energy densities but low power delivering density. On the other hand, conventional capacitors are capable of delivering high power densities but possess low energy storage density. Supercapacitors are a bridge between the two devices. Of all the types of supercapacitors available, electric double layer capacitors have promising future applications in mobiles, cars, computers, etc.

The present thesis aims to gain deeper understanding of the electrical double layer mechanism of energy storage. In order to study the mechanism, two aqueous electrolytes are considered: potassium hydroxide, and sulphuric acid. A computational approach is adopted to calculate the differential capacitance of the supercapacitor under various temperatures. The differential capacitances for the two different electrolytes under the same conditions are found to be characteristically different. An attempt has been made to relate these differential capacitance curves obtained to the structures of electric double layer for explanation. Finally, future scope of work for understanding electric double layer mechanism and enhancing current capability of storing energy in a supercapacitor is discussed.

Table of Contents

x

List of Illustrations

xiv

List of Tables

Chapter 1

INTRODUCTION

One of the most critical issues that human race is facing is that of energy crisis. Depletion of oil is imminent in the near future. Other conventional sources of energy that are available are not clean sources of energy affecting our environment. A need has arisen to explore new non-conventional energy sources as well as novel ways of storing energy.

Currently, we are facing problems with producing, storage as well as distribution of energy. One of the problems with producing energy is regarding shortage of fossil fuels and the pollution caused in the process. Many non-conventional sources such as solar energy, wind energy and tidal energy are being explored. The diagram shown below gives current scenario about energy demand.
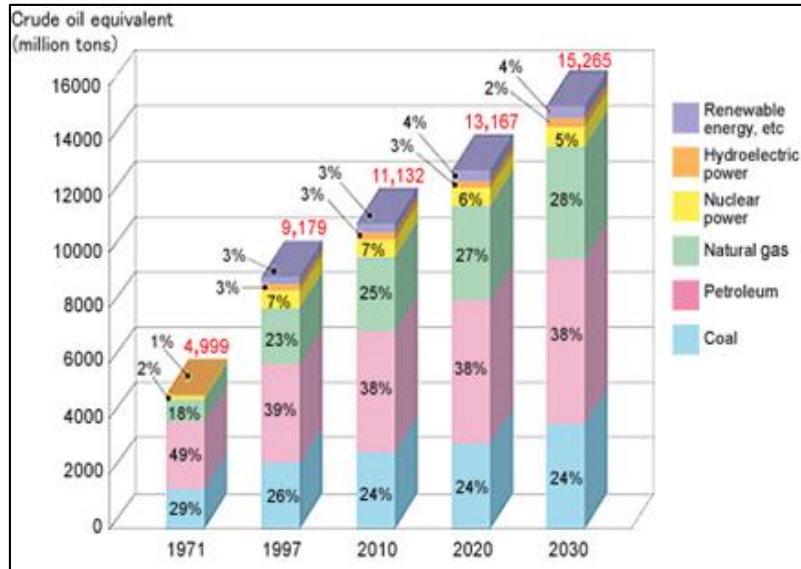
Figure 1.1 Energy Scenario [26]

Another problem is that of distribution of the produced energy. Generally fuels such as natural gas and oil are supplied by pipes to the destination. These fuels can then be stored at the location in tanks. Electric power is transmitted using transformers, high tension (HT) cables at high voltage and then it is stepped down to the usable voltage at local distribution centers. However, today if we look at devices such as electric vehicles mobile phones, laptops and computers, a need has emerged to store the electrical energy in the device and then utilize it over a period of few hours or days. This is where various energy storage devices such as non-rechargeable batteries, rechargeable batteries, capacitors, supercapacitors (ultracapacitors) come into picture. [2]

1.1 Energy Storage Devices

1.1.1 Battery

Currently, batteries are the most commonly used devices for electrical energy storage. Batteries are being used in a wide variety of applications such as automobiles, home appliances, electric locomotives and heavy duty fork lifts. Battery systems are used in photovoltaic arrays for storing the power during day time and supplying power during peak periods.

Some types of rechargeable batteries are Lithium-Ion, Nickel-Cadmium and Lead-Acid. Charging can take a few minutes or even few hours. This typically depends on the voltage; which when higher charges the battery faster but

can damage it as well. This slow charging is one of the drawbacks of currently used batteries. A typical battery is shown below:

Figure 1.2 Batteries [13]

Batteries store energy at higher density than other devices such as capacitors. The typical value for a non-rechargeable battery ranges between 90 and 455 Wh/kg; while for a rechargeable Ni-Cd battery it is around 230 Wh/kg. However, the power density of batteries is low (less than 0.1 kW/kg) [14]. A battery can supply power at low density for long time. Apart from this, life cycle is short and hence batteries cannot be used for light weight applications. [3]

1.1.2 Capacitors

Capacitors store electrical energy by the virtue of electric field. Capacitors have very high power densities than batteries ranging between 10^2 and 2.7 x 10^7 kW/kg. [3] Conventional capacitors have very high life with over 10,000 life cycles as compared to only 1000 for batteries. However, the energy storage density is very low (less than 0.05 Wh/kg) [3]. This is a very significant drawback

for many applications which require the energy to be stored for a long period and hence are not very widely used. A device which could combine the characteristics of battery and a capacitor needed to be designed. Supercapacitor, also known as ultracapacitor is such device. [4]
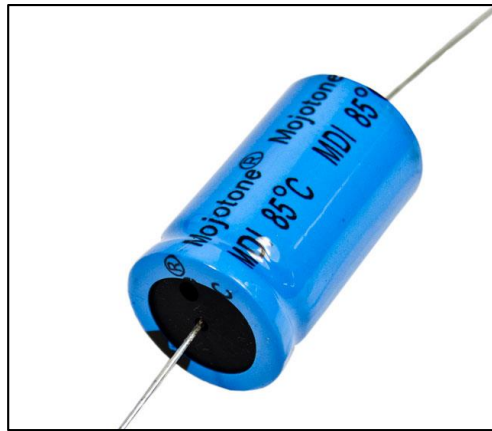
Figure 1.3 Conventional Capacitors [16]

1.1.3 Supercapacitors

These are electrochemical devices which primarily utilize high surface area electrode materials and thin electrolytic dielectrics to achieve very high capacitance of several orders compared to a conventional capacitor. It is hence possible to get higher energy density than a conventional capacitor and at the same time, achieving higher power density than non-rechargeable and rechargeable batteries.

The working of an ultracapacitor is in principle similar to working of a conventional capacitor. It has been discussed in detail. A capacitor consists of two conducting electrodes separated by a dielectric material. On application of voltage

4

on the electrodes, opposite charges are developed on the surface of electrodes. However, these charges remain separated from each other due to dielectric material in between them. As a result, electric field is created which stores the energy developed. [3]

Capacitance is given by,

$$C = \frac{Q}{V}$$

Here, Q is the stored charge when a voltage V is applied. Thus, capacitance is directly proportional to the surface area of each electrode and varies inversely with the distance D between the electrodes. [3]

Capacitance can also be given as,

$$C = \varepsilon_0 \varepsilon_r \frac{A}{D}$$

Here, ε is the constant of proportionality; which is a product of permittivity of free space and the dielectric constant of the separating material. [3]

Two main parameters i.e. Energy density and Power density can be calculated as a quantity per unit mass. The energy stored in a capacitor is given by,

$$E = \frac{1}{2}CV^2$$

Power is calculated per unit time. For calculating power, capacitors are connected in series in a circuit and some load resistance is added as well.
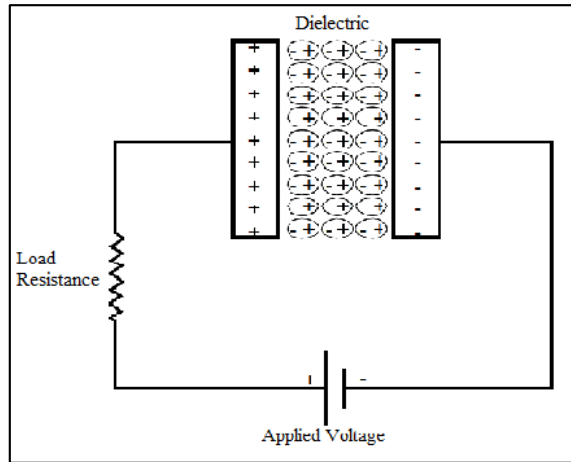
Figure. 1.4 Capacitor Schematic [19]

The equivalent series resistance (ESR) takes into account the internal resistances of all components. The maximum power is given as

$$P_{max} = \frac{V^2}{4 \; X \; ESR}$$

As mentioned earlier, supercapacitors being governed by the above stated equations, very high capacitance and hence energy density can be obtained by increasing the surface area and minimizing the separation distance. At the same time, high power density can be obtained by achieving very low ESR characteristic similar to a conventional capacitor. [3] [18]

The figure shown below, called the Ragone plot gives us a brief idea about energy and power densities for various electrical energy storage devices. As clearly seen, Supercapacitors Bridge the gap between devices such as batteries and fuel cells and conventional capacitors. [3] [18]

Figure 1.5 Supercapacitor [17]
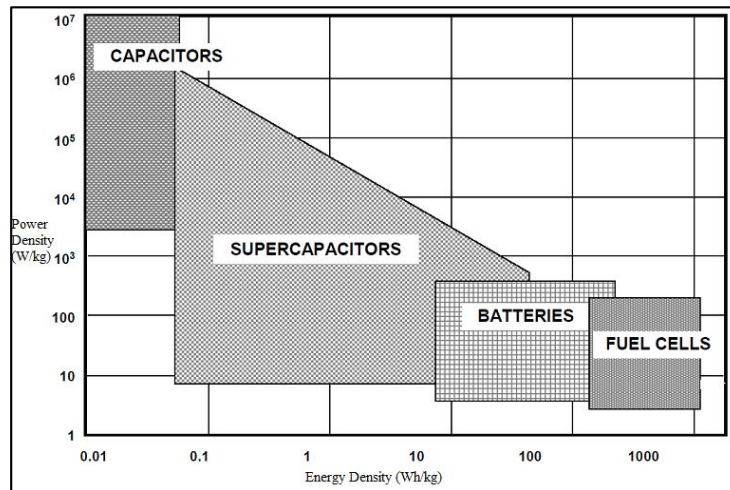
Figure 1.6 Ragone Plot [3]

Parameters	Capacitors	EDLC	Batteries
Energy Density (Wh/kg)	0.1	3	100
Power Density (W/kg)	10^7	3000	100
Time of Discharge (s)	10^{-3} to 10^{-6}	0.3 to 30	> 1000 to 10000
Cyclability	10^{10}	10^6	1000
Lifetime (Years)	30	30	5
Efficiency (%)	>95	85-98	70-85

Table 1.1 Comparison of Energy Storage Devices [3]

1.2 Taxonomy of Supercapacitors

Supercapacitors can be divided into three main categories: (i) Electrochemical Double-Layer Capacitors, (ii) Pseudocapacitors and (iii) Hybrid Capacitors. EDLC's involve Non-Faradic processes of energy storage. The charges are distributed on the surfaces physically and no breaking of chemical bonds is involved. Faradic mechanism involves intense reduction and oxidation reactions between electrode and electrolyte, which causes energy storage. The third type constitutes a combination of both mechanisms. [3]
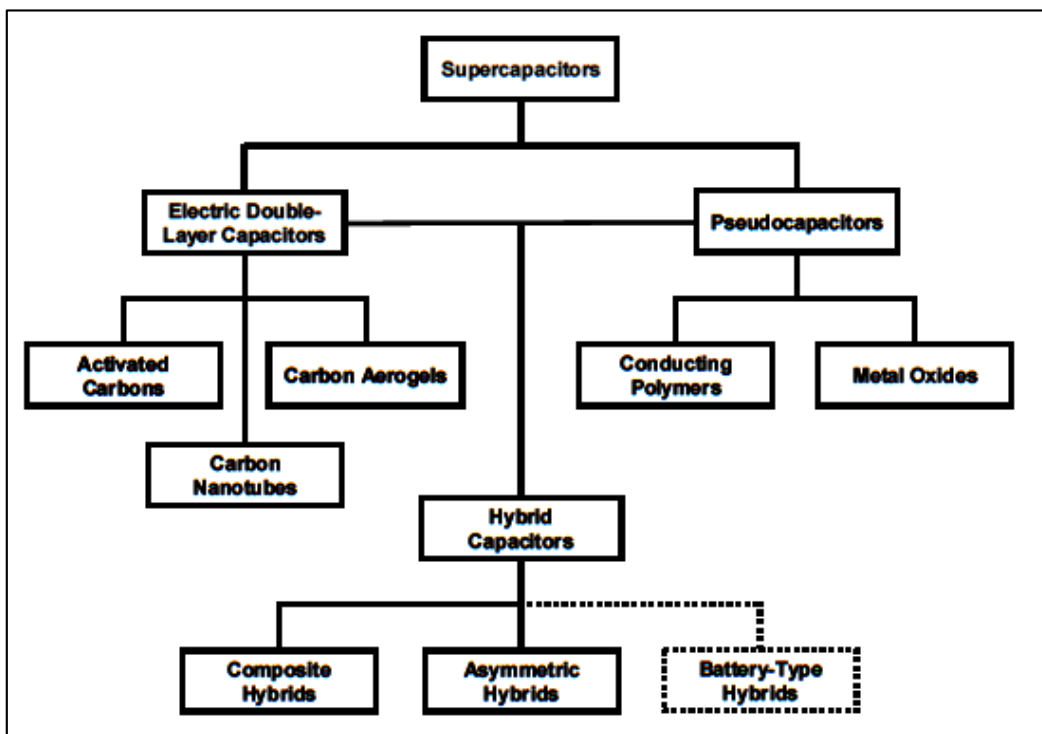
Figure 1.7 Taxonomy of Supercapacitors [3]

Let us consider each type of ultracapacitor and discuss every sub type in detail.

1.3 Electric Double Layer Capacitor

EDLC's comprise of two electrodes which are generally carbon based; such as Carbon Nanotubes, Activated Carbons and Carbon Aerogels. These devices store energy electrostatically as discussed above. There is no transfer of charge from electrode to electrolyte and vice-a-versa.

As voltage is applied, charge accumulates on the electrode surfaces. Opposite charges i.e. ions attract each other and then they diffuse in the solution and then into the pores of electrodes of opposite charge. The electrodes are constructed in such a way that recombination of ions does not take place. Thus, a double layer is produced at each electrode. These double layers provide an increase in surface area and a decrease in the distance between electrodes, giving higher densities. [16]

As this process is Non-Faradic, the energy storage is highly reversible, allowing the device to achieve high cycling stabilities. A very high number of charge and discharge cycles, up to 10^6 is also obtained [4]. On the other hand, batteries have up to 1000 charge and discharge cycles. Another important characteristic is that the performance of a supercapacitor can be altered by changing the electrolyte. EDLC's generally use aqueous and organic electrolytes [15] [16]. There are some advantages and disadvantages of these electrolytes and those shall be considered in the section discussing in detail about electrolytes. Now let us have an overview of each type of electrode.

1.3.1 Activated Carbons

This is the most commonly used electrode material owing to its higher surface area and less cost. They have various pore sizes with micropores (< 20 Å), and mesopores (20-500 Å) and macropores (> 500 Å) [3]. Although theoretically the capacitance varies directly as area, empirical data shows that discrepancies are caused when electrolyte ions that are very large are diffused in to micropores, preventing charge storage. Hence, larger pores give higher power densities and smaller pores give higher energy densities. Hence, this is a very important area for research researchers are trying to find optimal pore sizes and their size control during fabrication. [4]

1.3.2 Carbon Aerogels

Carbon aerogels are formed from a continuous network of conductive carbon nanoparticles with interspersed mesopores. This material has the ability to bond to current collector, eliminating the need of an adhesive binding agent. Due to absence of binding agent, ESR is drastically reduces, there by yielding more power density. This is very important factor for supercapacitors. [3]

1.3 3 Carbon Nanotubes

This is the most researched material for supercapacitor electrodes. Electrodes made from CNT's are generally grown in the form of a mat. Mesopores are open and easily accessible. In CNT's, mesopores are interconnected allowing a uniform charge distribution and also uses the complete

available surface area. The electrolyte ions easily diffuse in the mesoporous network and hence the electrodes possess low ESRCNT's can be grown directly onto collectors, treated or grown on colloidal suspension thin films. [3]
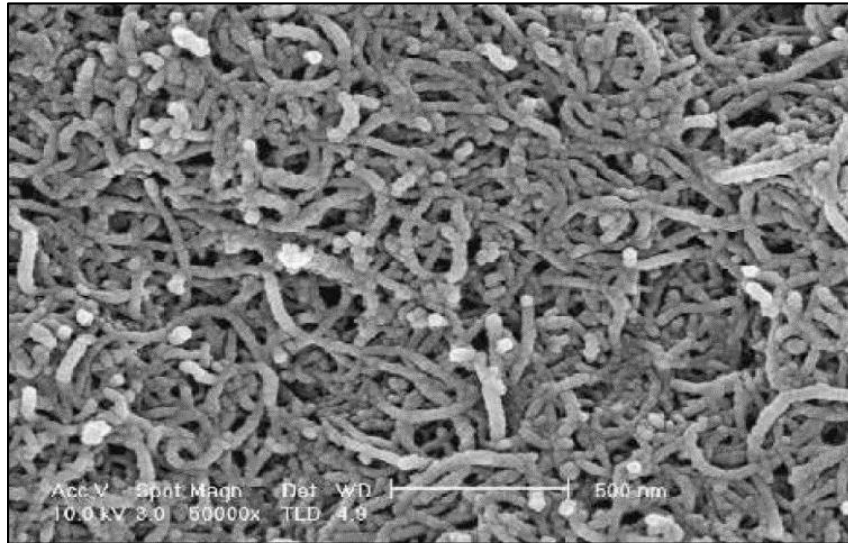
Figure 1.8 Carbon Nanotubes Microscopic View [3]

1.4 Pseudocapacitors

These ultracapacitors store charge as per Faradic process, which is through chemical reactions and not electrostatically as in case of EDLC's. The reactions are generally reduction-oxidation reactions. These processes allow greater capacitance and high energy densities. These devices are divided in to two categories; conducting polymers and metal oxides. [3]

1.4.1 Conducting Polymers:

These materials have high conductivity, high capacitance and low ESR as compared to the previous carbon related materials. In this configuration, one

polymer is positively (p) doped while the other is n-doped. P-doped polymers possess greatest potential energy and energy densities. However, n-doped polymers are very rare to get. This has hampered the development of such capacitors. Apart from this, redox reactions cause considerable mechanical stress on the electrodes and limits the stability of Pseudocapacitors over a period of many charge and discharge cycles and is one of the factors hampering the development of these devices. Some of the examples of polymer materials are polyaniline, polypyrrole and polythiophene. [3]

1.4.2 Metal Oxides

Metal oxides have been explored owing to their high conductivity. Some of the examples MnO_2, V_2O_5, RuO_2, etc. [5]. The majority of the research is directed towards ruthenium oxide. The reason behind this is the high level of capacitance that can be obtained as compared to other metal oxides. The capacitance is due to insertion and removal or intercalation of protons into amorphous structure. In hydrous form, the capacitance exceeds the one obtained by carbon based materials or polymers. The ESR of this metal oxide is lower than any material we previously reviewed, thus giving better energy and power densities. In spite of all these advantages, cost is a major issue. Major research is directed towards development of fabrication methods and composites which would enable us to obtain electrodes at less cost without affecting the performance. [3]

12

1.5 Hybrid Supercapacitors

These capacitors are designed in such a way that they eliminate the disadvantages of EDLC's and Pseudocapacitors and combine the advantages of both. They utilize Faradic as well as Non-Faradic mechanisms to store charge, enabling to achieve energy and power densities better than EDLC's and affordability and cycling stability of Pseudocapacitors. There are three types of such ultracapacitors (i) Composite, (ii) Asymmetric and (iii) Battery type. [3]

1.5.1 Composite

These electrodes integrate carbon-based materials with either a polymer or metal oxide and incorporate the storage mechanisms of both; physical and chemical. Carbon based materials develop double layer and provide a high-surface-area support that increases the contact between the deposited pseudocapacitive materials and electrolyte. These materials are able to enhance the capacitance of the composite electrode through Faradic reactions. Such electrodes constructed from CNT's and polypyrrole have been successful. This can be achieved due to the mat structure of CNT's which allow uniform three-dimensional distribution of charge. The mechanical robustness is however low due to the mat. This limits the mechanical stresses that the structure can take due to the insertion and removal of ions in deposited polypyrrole. These materials show the cycling stability comparable to EDLC's. [2] [3]

13

1.5.2 Asymmetric

These electrodes are formed by coupling an EDLC electrode with a pseudocapacitor electrode. As discussed earlier, there is a problem finding an n-doped polymers and hence this can be overcome by using activated carbons instead of the polymer. These polymers have higher capacitance but lower maximum voltages and cycling ability than the activated carbons. [2] [3]

1.5.3 Battery Type

These devices couple two different electrodes. The peculiar characteristic is the coupling a supercapacitor electrode with a battery electrode. This gives a combined effect of higher energy density as well as higher power density. The cycle life and recharging times are that of a supercapacitor, meaning less time and more operational cycles. Currently research is focused towards using nickel hydroxide, lead oxide and LTO ($Li_4Ti_5O_{12}$) as one electrode and activated carbon as the other. [2] [3]

1.6 Electrolytes

Electrolytes are composed of various solvents containing salts. The electrolytic system must exhibit good conductance and power output, good ionic adsorption and good dielectric constant value, which determines double layer capacitance and its dependence on electrode potential as well as the extent of ionization or ion pairing of the solute salt, which affects overall conductance. An

ideal electrolyte must possess high ionic conductivity, wide voltage range, low viscosity, low toxicity, low cost, thermal stability and high electrochemical stability. There are three types of electrolytes used (i) Aqueous Electrolytes, (ii) Organic electrolytes and (iii) Ionic liquids. Let us consider each type of electrolyte in detail.

1.6.1 Aqueous Electrolytes

The most commonly used electrolytes are sulphuric acid (H_2SO_4) and potassium hydroxide (KOH) [9]. These electrolytes display high conductivity, yielding higher power density as compared to no aqueous electrolytes. There are other advantages such as low cost and easy manipulation for use. However, the use of these liquids is restricted by the thermodynamic window of water at 1.23V. [4] [6] However, a voltage of 2.2V has been achieved with some salts such as Li_2SO_4, Na_2SO_4 and K_2SO_4 [5]. Apart from this, exceptional cycling stability has also been observed. This has renewed interest of aqueous liquids for electrolytes. One problem encountered with these electrolytes is that of corrosion due to high electrochemical activity. This has slowed the commercialization of these devices. Research is being conducted for finding out electrolytes with neutral pH. [27]

1.6.2 Organic Electrolytes

These liquids are capable of yielding voltages higher than 2.8V and also higher energy densities than aqueous electrolytes [3]. The operating voltage however depends in impurities of components such as water and surface carbons.

15

Conventional electrolytes contain salts such as tetraethyl ammonium tetrafluoroborate and solvents such as acetonitrile (ACN) or propylene carbonate (PC). These salts are widely used owing to good conductivity and ability to dissolve in non-aqueous solvents. PC carbonates are in use extensively in Japan whereas, ACN is more popular in the USA and Europe. It has been observed that that PC- based electrolytes have lower conductivity giving lower power output. Apart from this, the decrease in capacitance is prominent at lower temperatures for PC than CAN. However, CAN has got a very low flash point, making it a dangerous choice. Generally, -40°C to 70°C is considered to be an optimum and safe range for operation. These electrolytes are most widely used in the industry. There are however, some disadvantages such as high cost, low dielectric constant, flammability and toxicity of the liquids. [27]

1.6.3 Ionic Liquids

Ionic liquids (IL's) are molten salts at room temperature. They consist purely of cations and anions. They show excellent properties for use in ultracapacitors due to high thermal stability (up to 300°C), almost zero vapour pressure, non-flammability, low toxicity, low corrosive action and wide voltage window ranging from 2 to 6V [27]. They have a well-defined ion size. They are not yet suitable for large-scale applications because of high cost, difficulty in maintaining purity and complex process of production. ILs researched for application in supercapacitor electrolytes are imidazolium, pyrrolidinium, as well

as asymmetric, aliphatic quaternary ammonium salts with anions such as tetrafluoroborate, trifluoromethanesulfonate, bis (trifluoromethanesulfonyl) imide, bis (fluorosulfonyl) imide [12]. These are generally used in conjunction with carbon electrodes, mainly for extreme climatic conditions. [27]

We thus discussed all the types of supercapacitors and electrolytes in brief. Let us now look at EDL Supercapacitor and its construction.

1.7 Construction of Supercapacitor

1.7.1 Cell Construction

The cell consists of two electrodes, a separator and an electrolyte. Electrodes are made up of a metallic collector, which is the high conducting part and of an active material with high surface area. The membrane or separator which separates the electrodes allows mobility of ions but forbids electronic conductance. Generally, this material is rolled or folded into a rectangular shape and then placed inside the container. The system is then filled with electrolyte. The working voltage of device is determined by the decomposition voltage of electrolyte, temperature, current intensity and required lifetime. [2] [3]

Separator

Most of the currently available separators have been designed for use in batteries. An accurate design of separator is needed to obtain high performance of supercapacitors. Generally with organic electrolytes, paper separators are used

whereas with aqueous electrolytes, ceramic or glass fiber separators are used. The separator allows the transfer of charged ions but prevents electronic contact between electrodes.

The basics of obtaining high capacitance is to have ionic conductance, high ionic separator conductance. High electronic separator resistance, large electrode surface, low separator and electrode thickness. [2] [3]
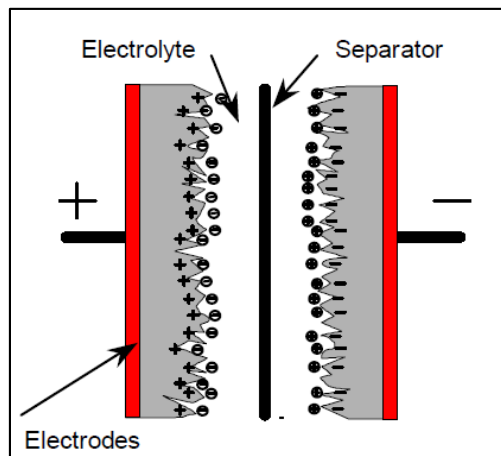
Figure 1.9 Supercapacitor Schematic [3]

1.7.2 Materials Research

Most of the research has been dedicated to development of materials on laboratory scale devices. Activated carbon composites and fibers with surfaces up to 3'000 m2/g, measured by gas adsorption, as well as carbon aerogels with surface areas up to 850 m2/g have been investigated. Unfortunately a significant part of the surface area resides micropores (<2nm) which are inaccessible to the

electrolyte ions [3]. The remaining surface area electrochemically accessible (meso and macropores) yields a capacitance well below the estimated values. Therefore the pore size distribution together with the surface area are important for the determination of the double layer capacitance. Since Iijima's original work, nanostructured materials such as carbon nanotubes have been recognized as a material with promising applications in chemistry and physics. Many methods were developed to synthesize nanotubes as arc-discharge process, chemical vapor deposition (CVD) i.e. pyrolysis of hydrocarbons, laser ablation and a variety of combinations of the above mentioned methods. Several requirements still remain to be fulfilled before the development of a nanotube-based technology, and in particular the production of macroscopic quantities of nanotubes can be achieved. [2]

1.7.3 Winding Technology

Many production and deposition methods exist to produce supercapacitor electrodes. The extrusion of charged polymers, produced by mixing activated carbon in a polymer matrix, is a possible way to produce good performance and low cost carbon electrodes for supercapacitors. The advantages of this process are a continued fabrication process resulting in a high productivity and therefore in low costs. The extruded carbon foil is very homogeneous, can be produced in variable sizes and is self-supporting. [2]

Advantages of the winding technology are a very reliable process, a high productivity and therefore low costs. This winding technology allows variable sizes and designs of the devices as the composite is subsequently rolled or folded into a cylindrical or debit card shape. Due to a good control of the foil tensions during the winding, it is possible to achieve a low ESR value. [2]

As we have now seen the construction of this device, we shall now consider in detail the actual mechanism that enables storage of energy. We will also briefly review the methods of analysis available for this mechanism.

1.8 Electric Double Layer (EDL)

EDL is developed on the surface of any object which is suspended in a fluid. The double layer is a structure consisting of two layers. The first layer is that which is formed the attraction of ions to the surface of the object. This may even be adhesive force. Thus, this layer is primarily a result of chemical interaction. This layer is firmly anchored to the surface and the charges/ ions do not move with respect to the surface. The second layer is formed when charges are attracted towards the first layer. In this layer, the ions are not fixed or anchored like the first layer, but are moving in the fluid. They are under the influence of thermal motion or electric attraction. This layer is called 'Diffuse' layer. [1] [2] [3] [11]
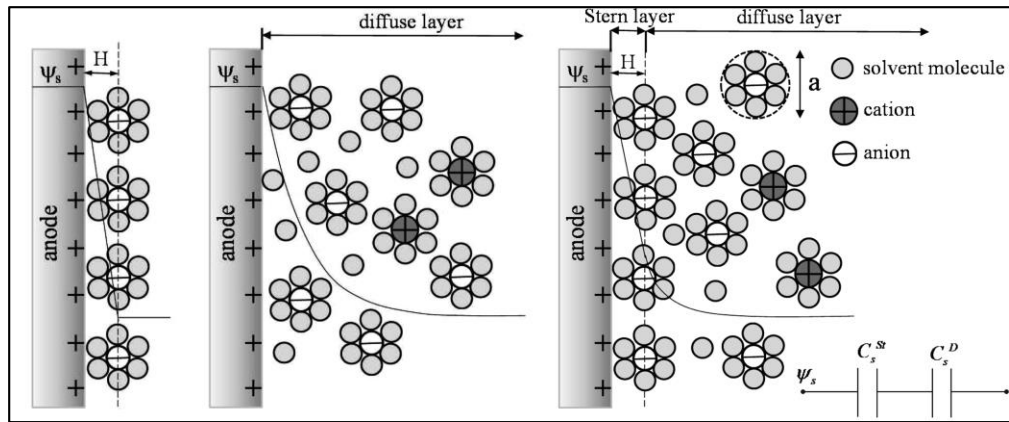
Figure 1.10 Electric Double Layer Structure [1]

The diffuse layer is a very peculiar phenomenon for bodies of very small size, that is at micro and nanometer scale. One such example is that of electrodes, which have very high surface area to volume ratio. [1] [2] [3] [11]

This is the principle used in development of Supercapacitors. As voltage is applied at the electrodes, energy is stored in the EDLC by the formation of closely spaced layers of charge at the interface formed between electrode and electrolyte. There lies some distance between the electrode and charged particles. This distance is in the scale of nanometers or Angstroms. This enables the system to generate a capacitance of very high magnitudes, which is far more than the conventional capacitors. EDL is related to Electrokinetic and Electroacoustic phenomena.

Electrokinetic phenomena occur as a result of a fluid containing particles such as gas bubbles and ions flowing over a flat surface. Electrophoresis is one such sub type of which deals with the study of motion of fluid particles under

influence of electric field. This phenomenon shall be considered in detail for our study. Electroacoustic phenomena occur as a result of ultrasonic sound waves propagating through a fluid containing ions. [1] [2] [3] [11]

Various models for studying EDL were established. We shall have an overview of each and then discuss the model of our study in detail.

1.8.1 Helmholtz Model

This one of the earliest models used to study the EDL phenomenon. Hermann von Helmholtz first theorized the concept of supercapacitor. It was he who noticed the formation of layer of ions on an oppositely charged electrode. At the same time, the electrodes would repel the likely charged i.e. co-ions. The two compact layers formed at the electrode-electrolyte interface were called 'electric double layer' (EDL). In this model, he also proposed that all the counter-ions would be adsorbed on the electrode surface. This he treated as a parallel plate capacitor. He proposed that the capacitance of such a system is inversely proportional to the thickness of the layer. He formulated the following equation for the model he proposed

Capacitance per unit surface area/Specific Capacitance, expressed in F/m^2 is given as follows:

$$C_S^H = \frac{\epsilon_0 \, \epsilon_r}{H}$$

$$C_S^H = \frac{\epsilon_0 \, \epsilon_r}{R_0 \log \left(1 + \left(\frac{H}{R_0} \right) \right)}$$

$$C_S^H = \frac{\epsilon_0 \epsilon_r}{H} (1 + (H/R_0))$$

Here, ϵ_0 and ϵ_r are the free space permittivity and the relative permittivity of the electrolyte solutions, respectively. H is the thickness of the double layer and approximated as radius of solvated ions. This was the first prediction of differential capacitance. He further believed that capacitance was independent of concentration of electrolyte and also surface potential. This was however, not proved in practice. This model also proposes that the differential capacitance depends on dielectric constant. [1] [2] [3] [11]

1.8.2 Gouy-Chapman Model

Gouy and Chapman independently developed a model for double layer. They both stressed the dependence of capacitance on electric potential and ion concentration. They proposed that the electrolyte ions did not perfectly separate in the solution to form Helmholtz layer. On the other hand, they proposed that there was a continuous distribution of charge along with concentrations of ions occurring near electrodes and decreasing away from the electrode. The model developed by Gouy and Chapman is based on Maxwell-Boltzmann statistics to take into account the ions' effect on each other. Thus, the most important consideration of these models was that they took into account the mobility of ions

and the combined effect of diffusion and electrostatic forces. Another important assumption is that ions are treated as point charges. The accuracy of these models was restricted to low charge densities at electrode-electrolyte interface. At equilibrium, the concentration is calculated using Boltzmann distribution as,

$$c_i = c_{i\infty} \exp(\frac{-z_i e \emptyset}{k_b T})$$

Here, z_i is the valency $c_{i\infty}$ is the bulk concentration of ion species i, k_b is Boltzmann constant, T is the absolute temperature and e is the electron charge. In this model, electric potential is calculated using Poisson-Boltzmann Equation, which is expressed as,

$$\nabla . (\in_0 \in_0 \nabla \emptyset) = 2ze N_A c_\infty \sinh\left(\frac{ze \emptyset}{k_b T}\right)$$

Here, N_A is the Avogadro's number. The equation above gives an exact solution when electrodes are planar and electrolyte properties are constant. The boundary conditions defined should be potential, $\emptyset(0) = \emptyset(D)$ and $\emptyset(\infty) = 0$. Then the specific capacitance is calculated for the diffuse layer as,

$$C_S^D = \frac{q_s}{\emptyset_D} = \frac{4ze N_A c_\infty \lambda_d}{\emptyset_D} \sinh\left(\frac{ze \emptyset_D}{2k_b T}\right)$$

Here, q_s is the surface charge density and λ_d is the Debye length. [1] [2] [3] [11]

1.8.3 Stern Model

Stern formulated a model for analyzing EDLC at high surface charge densities by combining the previous two models. According to Stern's theory, a

Helmholtz layer is present near the electrode surface and this layer transitions into a diffuse layer. The diffuse layer transition was governed by Maxwell-Boltzmann statistics. Grahame further improved the model by defining two layers of differing thicknesses. The Inner Helmholtz Plane (IHP) is formed by ions which are in direct contact with the electrode. The Outer Helmholtz Plane (OHP) is the layer formed by a solvation cell. This shell is made of polar solvent molecules that are attracted to the ion, increasing the radius. The solvation layer contains a solvent layer which separates the ion and electrode. The Figure 1.10 illustrates the models that we just discussed.

Let us now consider the effect of ion sizes on the model. Till now, ions were assumed to be point charges and the equations are valid for very low ion concentration. However, practically, ions have a size and the packing of ions defines the maximum concentration c_{max}. It is given by,

$$c_{max} = \frac{1}{N_A a^3}$$

According to Boltzmann distribution, the concentration does not exceed c_{max} and gives a surface potential of

$$\emptyset_{max} = -\left(\frac{k_b T}{z e}\right) \log(N_A \, a^3 \, c_\infty)$$

For Gouy- Chapman model and Gouy-Chapman-Stern Model, the magnitude of potential in the diffuse layer should be less than the maximum potential.

Of the many theories and models presented for taking into account the finite size of ion, Modified Poisson-Boltzmann equation is convenient to use mathematically as well as numerically. To make this model work, the concentration has to be restricted by using following expression,

$$c_i = \left(\frac{c_i^\infty \exp\left(\frac{-eZ_i\emptyset}{k_bT}\right)}{1 + 2v_i \sinh^2\left(\frac{-eZ_i\emptyset}{2k_bT}\right)} \right)$$

So this was an overview of the electric double layer models. In the next chapter, we shall formulate our own model for the study of electric double layer developed for better results than those given by previous model. [1] [2] [3] [11]

1.9 Objective

To study the relationship between Electric Double Layer structure and Differential Capacitance Curve in a supercapacitor.

Chapter 2

MATHEMATICAL MODEL OF EDL STRUCTURE AND PROBLEM

FORMULATION

These models have been established long ago. Our aim is to study the
transport phenomenon of transport (dynamics) of electrolyte when exposed to a
highly charged electrode. We also include the effects of electrostatic force, diploe
moment, entropic force and pressure. We shall base our theory on Fick's laws of
mass transport. For considering electrostatic forces and dynamic forces, Gauss's
law and Newton's laws are applied respectively. Let us now consider every aspect
in detail.

2.1. Chemical Potential

Let us consider an electrolyte on a charged surface. Electrolyte is a
mixture of freely moving ions and solvent molecules which can be polarized.
Chemical potential per particle can be used to describe the electrolytic system. It
is given by the equation,

$$\mu_i = k_B T \ln(n_i) + z_i e \phi - \int_0^{\tau_i} \nabla \phi \cdot d\tau_i + \gamma_i p \qquad (2.1)$$

Here, k_B is the Boltzmann constant, T is the temperature, ϕ is the
electrostatic potential, p is the hydrostatic pressure, e is the unit charge, and n_i,
z_i, γ_i and τ_i are the number concentration, the valance number, the chemical
expansion volume, and the induced dipole moment of the ith component,
respectively. The index i covers the individual constituents which include ions

27

and solvent molecules. First term in the equation represents the effect of entropy, second represents effect of charge, third term represents effect of dipole moment and the remaining gives mechanical pressure. [8] [20] [21]

The nonlinear polarization which take place at high voltage can be solved using Langevin equation. This equation can give polarization of solvent molecules and ions carrying permanent dipole moment, i.e. the separation which occurs due to two molecules of different electronegativity which causes unequal attraction of oppositely charged particle. The equation is given as,

$$\boldsymbol{\tau}_i = -\epsilon_0 \chi_i \nabla \phi$$

Where,

$$\chi_i \equiv \frac{3}{\bar{\tau}_{0i} E} \left(\coth(\bar{\tau}_{0i} E) - \frac{1}{\bar{\tau}_{0i} E} \right) \chi_{0i} \qquad (2.2)$$

And,

$$\bar{\tau}_{0i} = \frac{\tau_{0i}}{k_B T},$$

Here, ϵ_0 is the permittivity of vacuum, χ_{0i} and τ_{0i} are the linear polarization susceptibility per particle and the (permanent) dipole moment per particle of the ith component and $E = |\nabla \phi|$. Langevin equation is applicable only to orientation polarization of permanent dipoles. However, we have applied this equation to study linear electric susceptibility χ_{0i}, which gives us the degree of polarization of a dielectric material on the application of electric field [20] [21]. Substituting Eq. (2.2) in the third term of Eq. (2.1) and integrating, one obtains,

$$-\int_0^{\tau_i} \nabla \phi \cdot d\tau_i = k_B T \left(\ln \left(\frac{\sinh \bar{\tau}_{0i} E}{\bar{\tau}_{0i} E} \right) - \bar{\tau}_{0i} E \coth(\bar{\tau}_{0i} E) + 1 \right) \qquad (2.3)$$

2.2. Dynamic Transport and Field Governing Equations

Fick's laws are used to for predicting and analyzing the transport phenomenon of ions and molecules in a fluid. According to Fick's first law, flux for i^{th} species is expressed as,

$$\boldsymbol{j}_i = -M_i n_i \nabla \mu_i$$

Here, M_i is the mobility of ions, which may not be a single numerical but a complex function which considers concentration of all components. By substituting Eq. (2.1) in the above equation, and substituting the value of $D_i = M_i k_B T$ as per Einstein's relation, the equation for flux can be rewritten as,

$$\boldsymbol{j}_i = -D_i \nabla n_i + n_i \left[M_i \left(-z_i e \nabla \phi + \frac{\epsilon_0 \zeta_i}{2} \nabla (\nabla \phi \cdot \nabla \phi) - \gamma_i \nabla p \right) + \boldsymbol{u} \right] (2.4)$$

Here, $\boldsymbol{u}$ is the velocity, and electric field-dependent constant ζ_i is given by,

$$\zeta_i = 3 \left(\frac{1}{(\bar{\tau}_{0i} E)^2} - \coth^2(\bar{\tau}_{0i} E) + 1 \right) \chi_{0i} \qquad (2.5)$$

According to the law of conservation of mass, dynamic transport is represented by the equation,

$$\frac{\partial n_i}{\partial t} = -\nabla \cdot \boldsymbol{j}_i + R_i, \qquad (2.6)$$

Here, R_i is the production rate of a component through the chemical reaction. [10]

We shall now consider electrostatic potential and pressure gradient. We apply Poisson's equation for formulating the electrostatic potential.

$$\nabla \cdot \epsilon_0 (1 + \sum_i \chi_i n_i) \nabla \phi + \sum_i z_i e n_i = 0 \qquad (2.7)$$

Here, the second term is the summation of charge densities when separation of coions and counterions takes place. The value of field-dependent electric susceptibility is taken from Eq. (2.2). An important assumption is that the polarization effect is additive from all constituents. [22]

Now we formulate the governing equation taking into account the pressure effect. The electrolyte is assumed to be a compressible Newtonian fluid, implying that the stresses due to viscosity are linearly proportional to the strain rate. As per the Newton's law, equilibrium equation is given by,

$$-\nabla p + \nabla \cdot \eta \left(\nabla \boldsymbol{u} + \nabla^T \boldsymbol{u} - \frac{2}{3} \mathbf{I} \nabla \cdot \boldsymbol{u} \right) - \sum_i z_i e n_i \nabla \phi + \frac{1}{2} \epsilon_0 \sum_i \zeta_i n_i \nabla (\nabla \phi \cdot \nabla \phi) = 0$$

$$(2.8)$$

Here, p is the hydrostatic pressure caused due to elastic deformation. Second term in the equation represents viscous flow. The third and fourth terms represent electrostatic charge force density and electrostatic polarization respectively. Generally, Maxwell's tensor is used to calculate the electrostatic charge density, which is given as the divergence of Maxwell's stress. However, we have used Korteweg-Helmholtz method to calculate the electrostatic polarization force density of Langevin dipoles. The present electrical force density is derived directly from Eq. (15) in Sec. 3.7 in reference [20]. The third term representing polarization force is reduced to the Kelvin force density

$\left(\equiv \frac{1}{2}\epsilon_0 \sum_i \chi_i n_i \nabla(\nabla\phi \cdot \nabla\phi)\right)$ when $\bar{\tau}_{0i}E \ll 1$. However, the Kelvin's force density is not applicable in our case of Langevin's diploes which is of nonlinear nature. This happens because the microscopic forces experienced by individual induced dipoles (averaged) are not linear when added to consider at macroscopic level. [22] [23]

Hydrostatic pressure is a rate independent parameter and expressed as $p = p(N, V, T)$, where $N(\equiv \sum n_i)$ is the particles per unit volume. Packing density is given by $V(\equiv \sum v_i = \sum n_i\gamma_i)$. The Carnahan-Starling EOS for repulsion and Van der Waals attraction term is adopted. It is given as,

$$\frac{p}{Nk_BT} = \frac{1+V+V^2-V^3}{(1-V)^3} - \frac{a}{k_BT} \qquad (2.9)$$

Here, $a = \sum n_i a_{ij} n_j$, where a_{ij} is the attractive interaction effect between species i and j. Multi component mixtures are considered and then effective interaction is generalized, with $a_{ij} = \sqrt{a_{ii}a_{jj}}$. [22] [23]

2.3. Finite Volume Method

A finite volume method has been adopted to numerically solve the above set of governing equations (Eqs. (2.6)- (2.9)) along with appropriate initial-boundary conditions for fields n_i, ϕ, $\boldsymbol{u}$ and p in one-dimensional planar problems of an EDL. As per finite volume method, the first step was to present the problem of a divergence equation governing a field over a domain with surface integrals of

flux according to the divergence theorem. This we applied to each one of the cells (i.e., finite volumes) used to discretize the whole domain. The flux at cell boundaries was then approximately evaluated from nodal values of a field defined within the cells. When the flux (approximate), was applied identically to adjacent cells sharing the surface where it is defined, the law of conservation of the field quantity gets satisfied. Since the present multi-physics problem was highly nonlinear, an iterative scheme was indispensable.

We then discretized a one-dimensional finite domain into M cells, numbered in order from 1 to M. Each cell was assigned with a node at the middle point. Potential ϕ, concentration n_i and velocity $\boldsymbol{u}$ are the basic quantities, and are defined on the nodes. There are M nodal degrees of freedom for either one of ϕ, n_i or $\boldsymbol{u}$. Thus, one needs to gather M algebraic equations to solve for each one of them. This is attained by applying equations (2.6)-(2.8) to each cell. Based on the nodal values, the fields of ϕ, n_i and $\boldsymbol{u}$ near a knot m are approximated as

$$\phi(x; x^m) = \sum_q N_q^m(x)\phi_q, \qquad (2.10a)$$

$$n_i(x; x^m) = \sum_q N_q^m(x)n_{iq}, \qquad (2.10b)$$

$$\boldsymbol{u}(x; x^m) = \sum_q N_q^m(x)\boldsymbol{u}_q, \qquad (2.10c)$$

Here, superscript m indicates the mth knot, subscript q indicates the qth node selected to approximate the field around knot m, and $N_q^m(x)\left(= \prod_{p \neq q}\left(\frac{x-x_p}{x_q-x_p}\right)\right)$ is the Lagrange interpolation function in terms of selected nodal coordinates around

knot *m*. In later numerical examples, two nodes from the left side and two nodes from the right side, if available, were chosen to approximate a field about a knot. For knots near the ends (i.e., domain boundary), lower-rank interpolation is used, since there may be less than two nodes available on the end side. Derivatives and integrals of these fields around a knot can be conveniently obtained from Eq. (2.10). For the sake of brevity, their explicit expressions are not presented here.

By applying the divergence theorem, the governing equation of electrostatics (Eq. (2.7)) over the *m*th cell between knots *m*-1 and *m* is turned into

$$\epsilon^{m,l}(\phi_{,x})^{m,l+1} - \epsilon^{m-1,l}(\phi_{,x})^{m-1,l+1} + \sum_i z_i e n_{im}^l (\Delta x)_m = 0 \quad (2.11)$$

where $\epsilon^{m,l} \equiv \epsilon_0\left(1 + \sum_i \chi_i^{m,l} n_i^{m,l}\right)$, valid for $\epsilon^{m-1,l}$ as well, $(\Delta x)_m$ is the cell size, superscript l after comma indicates the lth iterative step, and subscript comma indicates partial differentiation with respect to the indices that follow. Again, superscript *m* (or *m*-1) in the first two terms indicates that ϵ and $\phi_{,x}$ are evaluated at knot *m* (or *m*-1) based on nearby nodal values by Eq. (2.10) and its derivatives. For example, $(\phi_{,x})^{m,l+1} = \sum_q N_{q,x}^m(x = x^m)\phi_q^{l+1}$. By assuming that all quantities at the lth iterative step are known, Eq. (2.11) offers an algebraic equation of unknown nodal values of potential at the $(l+1)^{\text{th}}$ iterative step.

Similarly, the governing equations of mass transport (Equations (2.4) and (2.6)) within the *m*th cell between knots *m*-1 and *m* are turned into

$$\frac{(\Delta x)_m}{\Delta t}\left(n_{im}^{l+1} - n_{im}^0\right) + \left(j_i^m - j_i^{m-1}\right) - (\Delta x)_m R_{im} = 0, \qquad (2.12a)$$

$$j_i^* = -D_i^{*,l}\left(n_{i,x}\right)^{*,l+1} + (A^{*,l} + u^{*,l})n_i^{*,l+1}, \text{ with } *= m, m-1, \qquad (2.12b)$$

$$A \equiv M_i\left(-z_i e\phi_{,x} + \epsilon_0 \zeta_i \phi_{,x}\phi_{,xx} - \gamma_i p_{,x}\right), \qquad (2.12c)$$

where n_{im}^0 is the nodal concentration at the previous time step, and Δt is the time step. Though more complicated, Eq. (2.12) works the same as Eq. (2.11) to offer an algebraic equation of unknown nodal values of n_i at the $(l+1)^{th}$ iterative step given all quantities at the previous iterative step. Above p is computed from Eq. (2.9). The time rate-of-change term in Eq. (2.6) is treated above as a source term with time-marching step Δt. Meanwhile, all other terms/quantities involved in Eq. (2.4) of j_i are evaluated at the current time step; thus, an implicit finite difference scheme is used to treat the temporal dynamics of the problem. [24]

Furthermore, the equilibrium equation of force balance (Eq. (2.8)) over the mth cell between knots m-1 and m are turned into

$$-(p^{m,l} - p^{m-1,l}) + \frac{4}{3}\left(\eta^{m,l}\left(u_{,x}\right)^{m,l+1} - \eta^{m-1,l}\left(u_{,x}\right)^{m-1,l+1}\right) + (\Delta x)_m f_m = 0,$$

$$(2.13a)$$

$$f = -\sum_i z_i e n_i \nabla\phi + \frac{1}{2}\epsilon_0 \sum_i \zeta_i n_i \nabla(\nabla\phi \cdot \nabla\phi). \qquad (2.13b)$$

This set of equations was solved for velocity field u at each iteration step.

Equations (2.11)-(2.13) are only applicable to interior cells. For boundary cells, the quantities evaluated at the knot at the boundary end should be replaced by a prescribed boundary condition. If a flux boundary condition is prescribed, the replacement is straightforward. If a potential/concentration boundary condition is

prescribed, it is converted into a flux boundary condition with a penalty coefficient. For instance, for diffusion at the far end (i.e., knot M), it is written: $j_i^M = k^M(n_i^M - \bar{n}_i^M)$, where k^M is the penalty coefficient, a numerical parameter, $\bar{n}_i^M$ is the prescribed value of concentration, and n_i^M is the concentration at knot M and expressed in terms of two nodal values next to the end by Eq. (2.10). If k^M is set sufficiently large, $n_i^M = \bar{n}_i^M$ is approximately obtained, with controlled, negligible numerical error. [24]

The solution procedure is briefly described as follows. Given appropriate initial and boundary conditions, the problem is solved incrementally in time and iteratively over each time step. Marching in time poses little issue in this case of a parabolic problem in nature. For each iterative step l+1, a system of algebraic equations with nodal potential ϕ_m^{l+1} as variables and all coefficients and other quantities evaluated from previous iterative step l is assembled from Eq. (2.11). The stiffness matrix is inverted to solve for nodal potentials at the $(l$+1)$^{\text{th}}$ iterative step. Then, nodal concentrations of the first chemical component at the $(l$+1)$^{\text{th}}$ iterative step is solved by inverting the stiffness matrix assembled from Eq. (2.12) with i =1. This is repeated until nodal concentrations of all chemical components are updated. Finally, Eq. (2.13) is solved to update velocity u. However, since the present problem is highly nonlinear, especially when concentrations reach their saturation values, this scheme with no relaxation may become unstable. Instead, the following over-relaxation scheme is used; for instance, for potential, $\phi_m'^{l+1} =$

$\phi_m^{'l} + \alpha\Delta\phi_m$, where $\Delta\phi_m$ is the difference of above obtained new value of ϕ_m from $\phi_m^{'l}$, and α is the relaxation factor. A larger α leads to faster convergence, but greater chance of numerical instability. Trials are needed to identify acceptable value of α. [24]

2.4 Problem Formulation

A supercapacitor consists of an electrode surrounded by electrolyte. The charge distribution is uniform at zero potential in all directions. Hence we can consider only one direction for our analysis and the problem can be hence reduced to One Directional Planar problem. This significantly simplifies the boundary conditions and problem solving.

We are considering aqueous electrolytes for analysis and hence the procedures from continuum mechanics are applicable for the analysis. KOH and H_2SO_4 are the electrolytes for our study. We shall consider electrodes made up of activated carbon of thin sheet. However, we restrict our study to the activities that occur in the electrolyte.
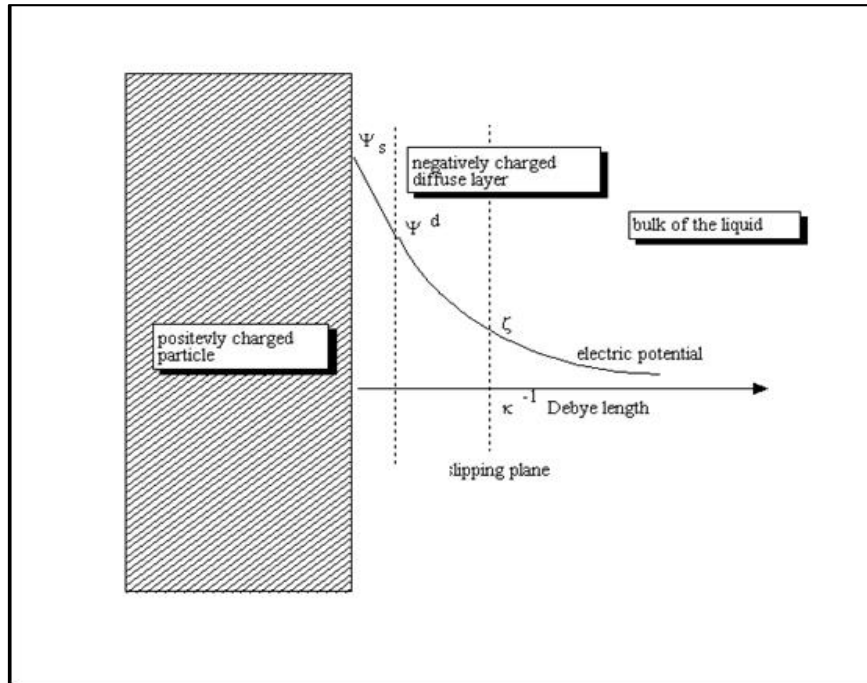
Figure 2.1 Problem Formulation [11]

At the electrode end, potential is present. It may be positive or negative. Potential is zero at infinite distance. However, flux is not applied for individual constituents in the electrolyte. No values of flux are hence entered in the code. Concentration remains constant at infinite distance. This problem is then solved using finite volume method that is mentioned above.

For our analysis, we studied the chemical reactions of dissociation of both electrolytes.
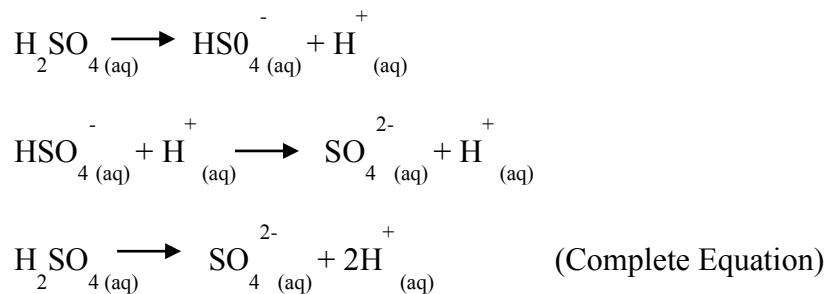
1. Reaction of KOH:

$$KOH_{(aq)} + H_2O_{(l)} \longrightarrow K^+_{(aq)} + OH^-_{(l)}$$
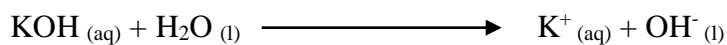
Here, the base splits clearly into two ions, cations and anions and thus dissociation is simple.

2. Reaction of H_2SO_4:

Sulphuric acid is a diprotic acid because it contains two ionisable hydrogen atoms. Hence dissociation of sulphuric acid take place in two parts. Image below shows the reactions.

$$H_2SO_{4\,(aq)} \longrightarrow HSO_{4\,(aq)}^- + H_{(aq)}^+$$

$$HSO_{4\,(aq)}^- + H_{(aq)}^+ \longrightarrow SO_{4\,(aq)}^{2-} + H_{(aq)}^+$$

$$H_2SO_{4\,(aq)} \longrightarrow SO_{4\,(aq)}^{2-} + 2H_{(aq)}^+ \qquad \text{(Complete Equation)}$$

We have considered the final complete reaction for our analysis. However, both the reactions should be included in study for more accurate model and results.

Chapter 3

NUMERICAL ISSUES

In this chapter, we shall review the numerical and physical issues and all factors that were considered for obtaining the results. The main aim of our research is the calculation of differential capacitance and study of parameters that are involved in the process of formation of double layer and diffusion of ions. This we have achieved by extensive mathematical simulation by inputting various parameters in the code and running trials. By varying voltage, relaxation factor, mesh size and truncation distance, we were able to reach the optimum value of all parameters. Then the obtained optimum voltage is applied to the electrode and various parameters are studied. Temperature is the important parameter which is varied to observe the capacitance and study the changes or processes going on in the double layer. This process is firstly applied to obtain the parameters for potassium hydroxide and then repeated for sulphuric acid.

For each of the electrolytes, parameters such as Stoke's radius, physical radius, permittivity etc. were plugged into the code to get the results. (Refer Appendix A)

3.1 Stoke's Radius

Calculation of Stoke's radius was done using the following relation:

$$R_H = a = \left(\frac{k_b T}{6\pi n D} \right)$$

Here,

k_b = Boltzmann Constant

T = Temperature in Kelvin

n = Viscosity of fluid

D = Diffusion constant

Thus, Stoke's radii were calculated for all the constituents. Rest of the properties were taken from standard data tables available. The table given below shows all the properties that were used and results were obtained.

Constituent	Physical Radius	Stoke's Radius	Permittivity
K^+	0.133	0.125	5.55
OH^-	0.153	0.0431	64.4
H^+	0.1552	0.0244	0
$SO4^-$	0.258	0.232	17.6
H20	0.1552	0.09687	79

Table 3.1: Physical Parameters of Electrolyte Constituents [7]

3.2 Debye Length Calculation

$$k^{-1} = \sqrt{\frac{\varepsilon_r \varepsilon_0 k_B T}{2 N_A e^2 I}}$$

Here,

k^{-1} = Debye Length

ε_r = Dielectric Constant

ε_0 = Permittivity of Free space

k_b = Boltzmann Constant

T = Temperature in Kelvin

N_A = Avogadro's Number

e = Elementary Charge

I = Ionic Strength in (mole/m^3)

3.3 Simulation Domain

3.3.1 Simulation Domain for Potassium Hydroxide

We shall first consider the electrolyte potassium hydroxide for our analysis. As we know, EDL and diffusion process in an electrolyte occur up to infinite distance. However, it is not possible to calculate the parameters at infinity. We thus need to truncate the distance from electrode to the point from where the activity becomes dormant or slow. This distance can be approximated using the Debye length of the electrolyte. However, this is only a rough estimate of truncation distance. During the trials, it was observed that the simulation domain taken as the value of Debye length proved insufficient to estimate and approximate the various phenomena occurring in the double layer. The Figure below shows the plots obtained when the simulation domain is taken as the Debye length (0.287nm). Input profile is provided in Appendix A.
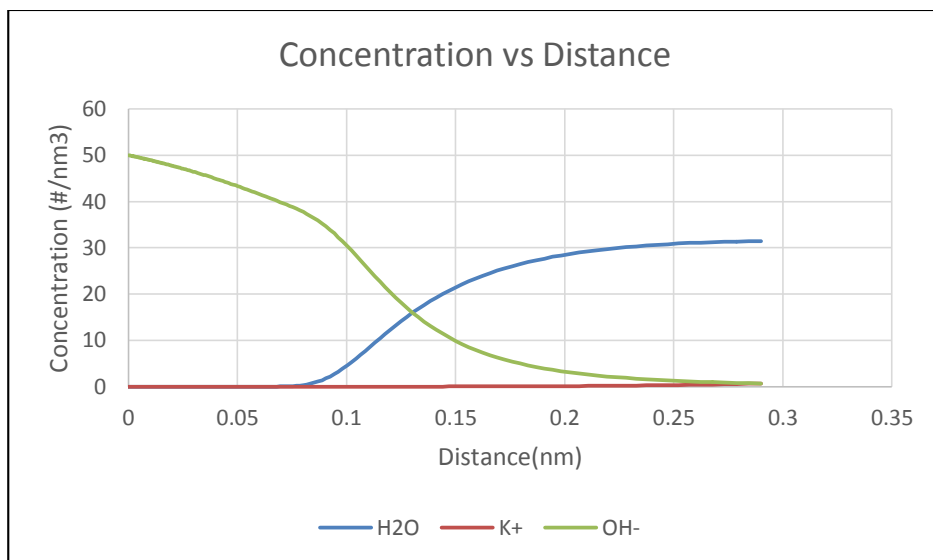
Figure 3.1 Concentration vs Distance for KOH (0.3 nm Simulation Domain)

As it can be seen here, the curves showing concentration of all constituents have a gradually increasing slope and the dissociation of the electrolytes is still ongoing. Hence this truncation distance is too less. This leads to inaccurate results. Thus, the simulation domain was increased up to 1.2 nm for analysis. This domain was too large and also the slope between 1nm and 1.2nm remained constant. Given below is the plot for this domain.
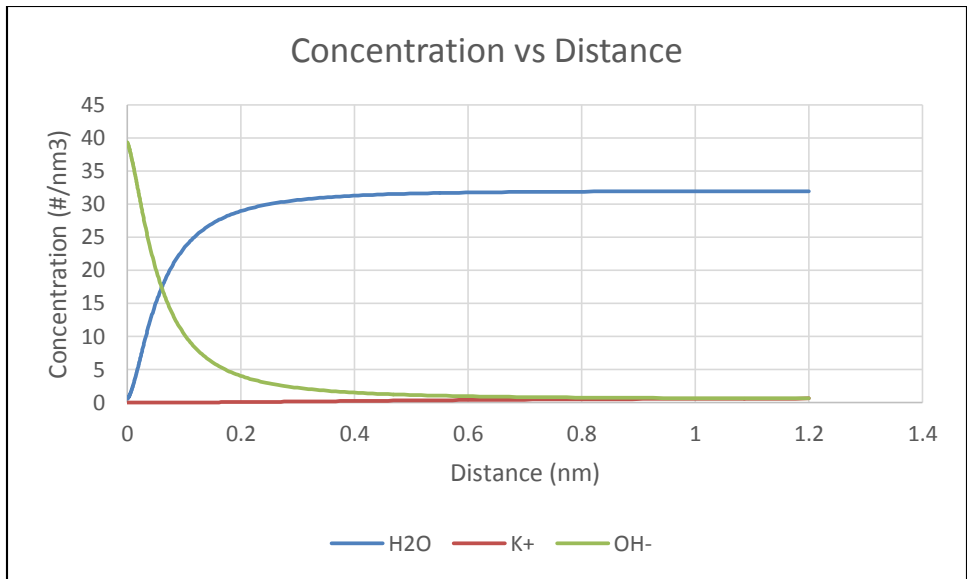
Figure 3.2 Concentration vs Distance for KOH (1.2 nm Simulation Domain)

The simulation domain was then changed to 1 nm and then analysis was carried out. The Figure given below shows the result for this domain.
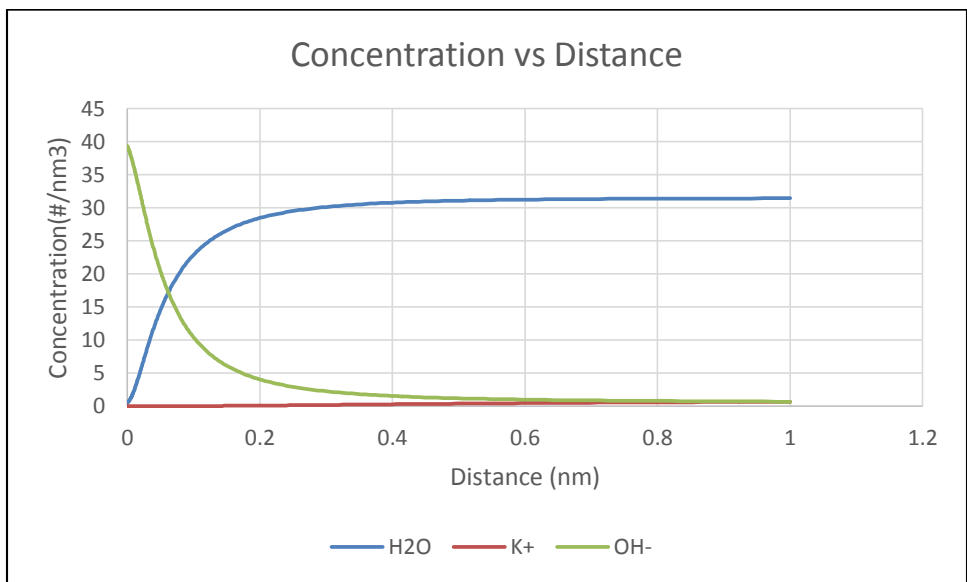

Figure 3.3 Concentration vs Distance for KOH (1 nm Simulation Domain)

3.3.2 Simulation Domain for Sulphuric Acid

As discussed for the previous electrolyte, truncation length was taken as Debye length and trial was taken to see if the simulation domain was sufficient for us to obtain desirable results. At first, the simulation domain was taken as 0.5nm and the plot obtained for this domain is shown below.
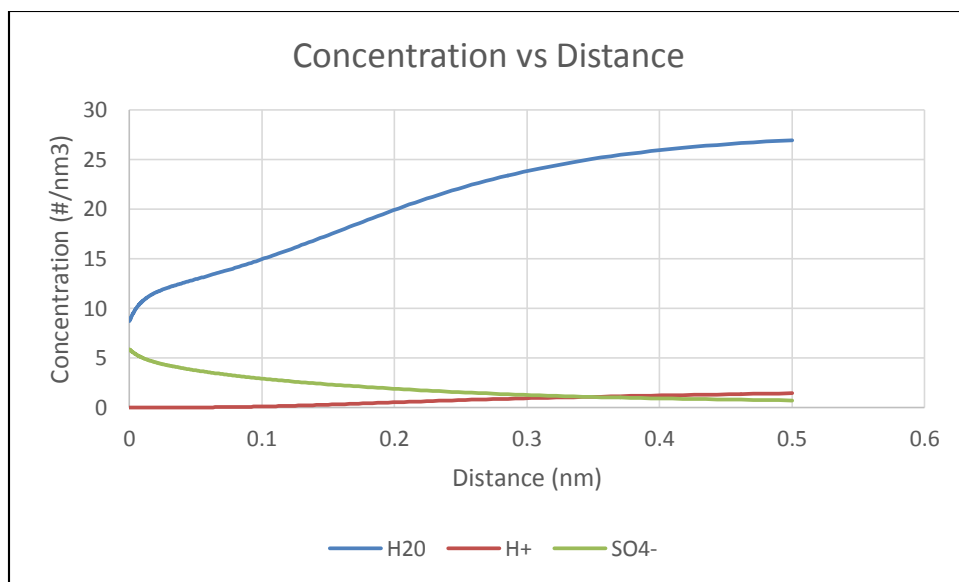

Figure 3.4: Concentration vs Distance for H2SO4 (Simulation Domain 0.5 nm)

Thus, as it can be seen, the process has not reached equilibrium and hence the domain had to be increased to 1 nm in order to get better results. The result is shown below.
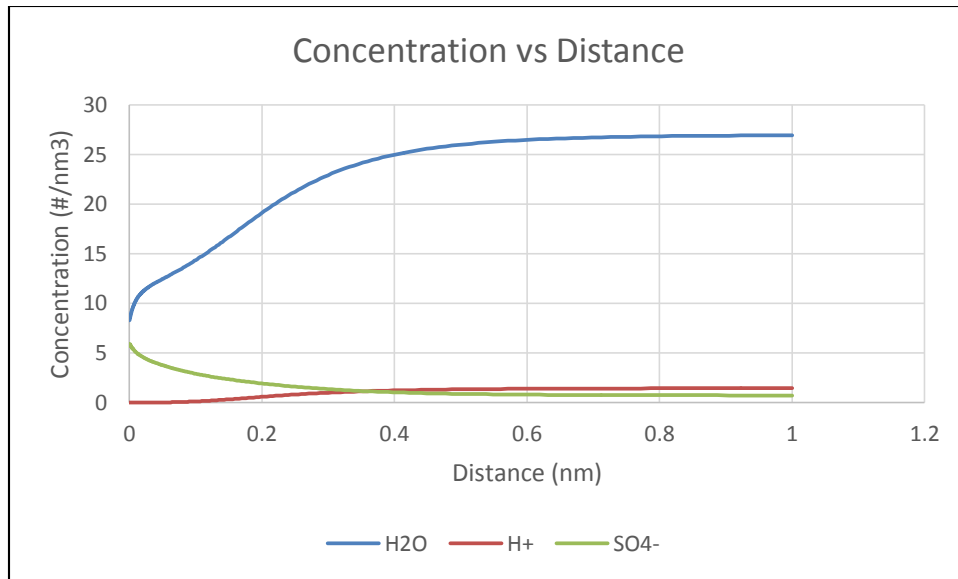
Figure 3.5: Concentration vs Distance for H2SO4 (Simulation Domain 1 nm)

This length was then used for further analysis of various parameters, which we shall review.

3.4. Voltage variation

3.4.1 Voltage variation for KOH as electrolyte

Initially voltage between the in the range of 0 to 2V in steps of 0.5V was applied to study the curves obtained against the distance of electrode. For these voltages, firstly, a graph of electrical displacement versus potential was obtained. The slope of this graph represents the differential capacitance obtained. These were just a trial runs to examine the differential capacitance curves obtained. One of the plots is shown below. As it can be seen, there is an increase in differential capacitance when the voltage is less than 0.1V. Then there is a gradual decrease in

the capacitance followed by very sharp decrease. This 'Camel-hump' shaped curve is the one obtained by the classical models of EDL formulation. The region between 0 to 0.2V is the one which we have to study for our research.
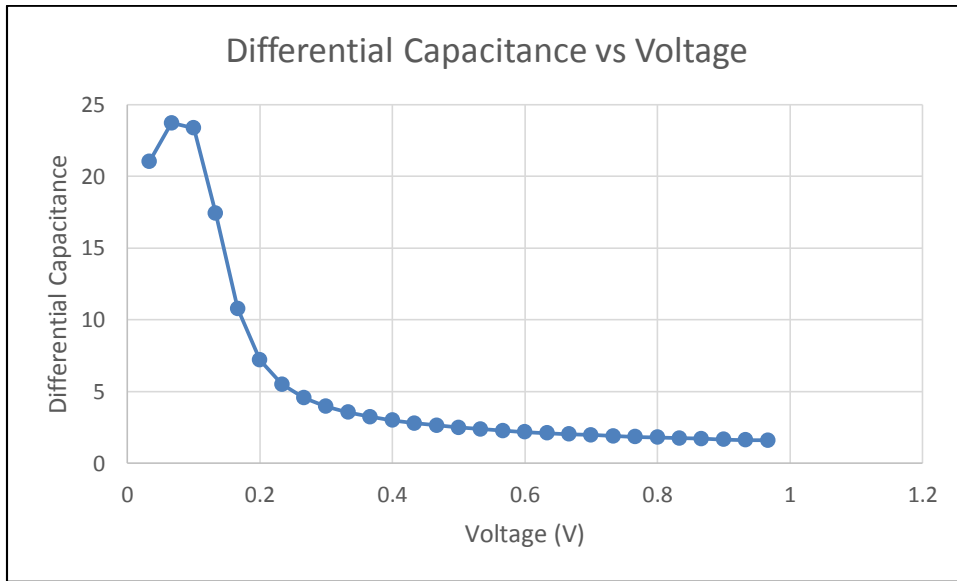

Figure 3.6: Differential Capacitance vs Voltage for KOH (1V)

For further analysis, we shall consider this voltage and study the differential capacitance against the parameters of our interest.

3.4.2 Voltage variation for H2SO4 as electrolyte

A process similar to one mentioned above was adopted to obtain the optimum voltage range for our study. The same code when run above 2V was giving errors and the solution values were not converging. So, voltage was increased in small steps. In this case, however, a hump-shaped curve was not obtained. By doing some trials, voltage of 0.2V was considered for doing further analysis and study the changes. One of the sample plot which is similar to KOH is

shown below. However, it can be seen that the camel-shape is not seen. This shape was not seen any of the trials done.
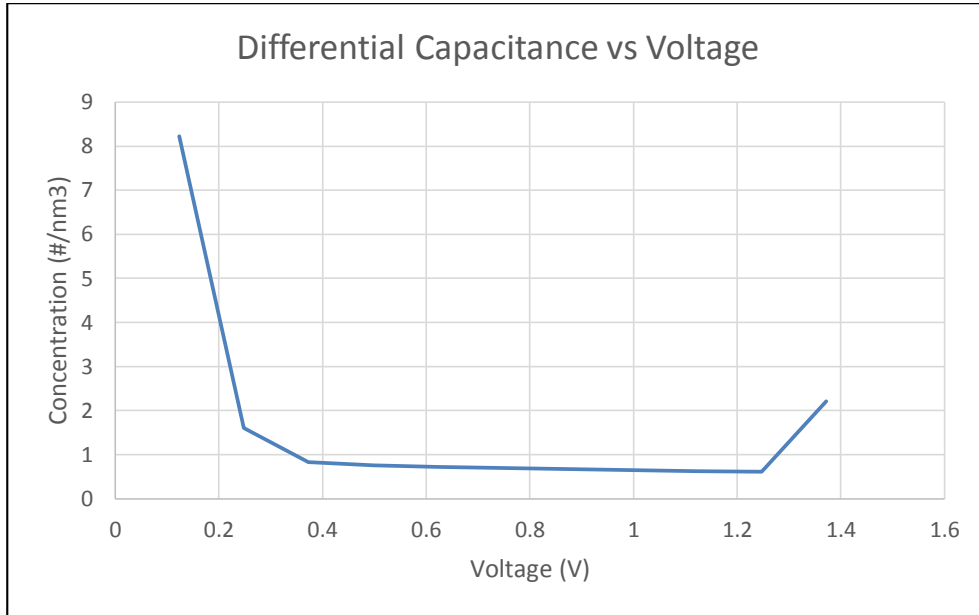

Figure 3.7: Differential Capacitance vs Voltage for H_2SO_4 (1.5V)

Once the voltage value was fixed, the same voltage was applied across a range of temperatures and then each parameter such as packing fraction, concentration, electric displacement and velocity were studied. Then a comparative study of these parameters against the temperatures was carried out for each electrolyte separately. One more thing considered for our study was that of application of negative voltage to study all the above mentioned parameters. Initial plot for differential capacitance is shown below.

3.5 Relaxation Factor

Relaxation factor plays an important role when the plots obtained are nonlinear. It also plays an important role in convergence of the solution. It was varied from 0.007 to 0.002 for which, acceptable plots were obtained.

3.6 Variation of Temperature

These capacitors are used in the temperature range above freezing point of water and 45°C. However, we have analyzed the parameters till 60°C i.e. 333K. In this case, initially step of 10K was considered. However, no major change was observed and hence, all the parameters have been observed and studied at 313K and 333K.

It is obvious that values such as permittivity, diffusivity, viscosity etc. change along with change of temperature. But Stoke's radius is an entity which remains constant over the temperature range that we are considering. This made our calculation easier.

3.7 Calculation of Differential Capacitance

Differential capacitance is the parameter for study Electric Double Layer For calculation of differential capacitance, a plot of electric potential and electric displacement is taken. The slope of this graph gives the differential capacitance, which is of our interest. Firstly, positive voltage was applied.
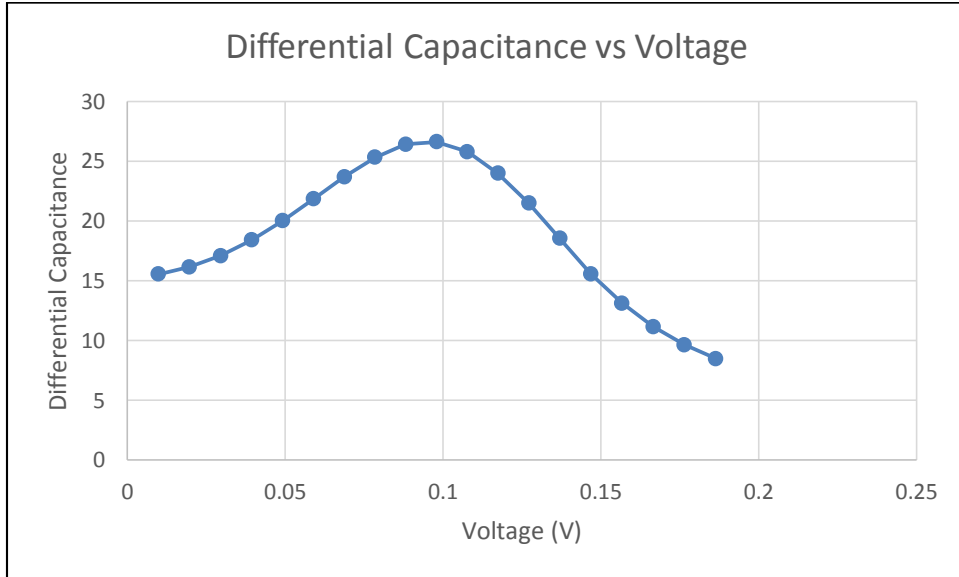
3.7.1 KOH as electrolyte

Figure 3.8: Differential Capacitance vs Positive Voltage (0.2V)

Similarly, plot for capacitance when negative voltage is applied is shown below.
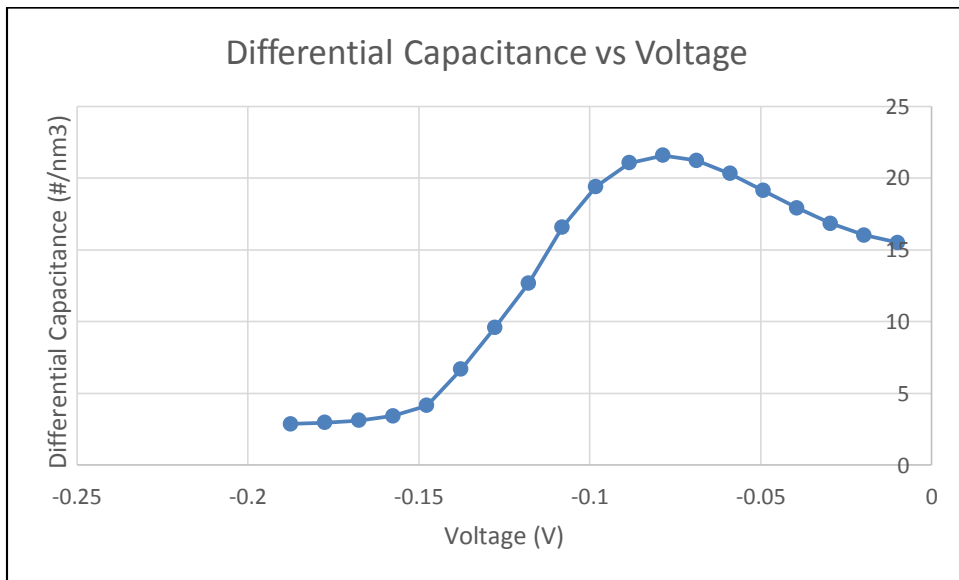

Figure 3.9: Differential Capacitance vs Negative Voltage (0.2V)
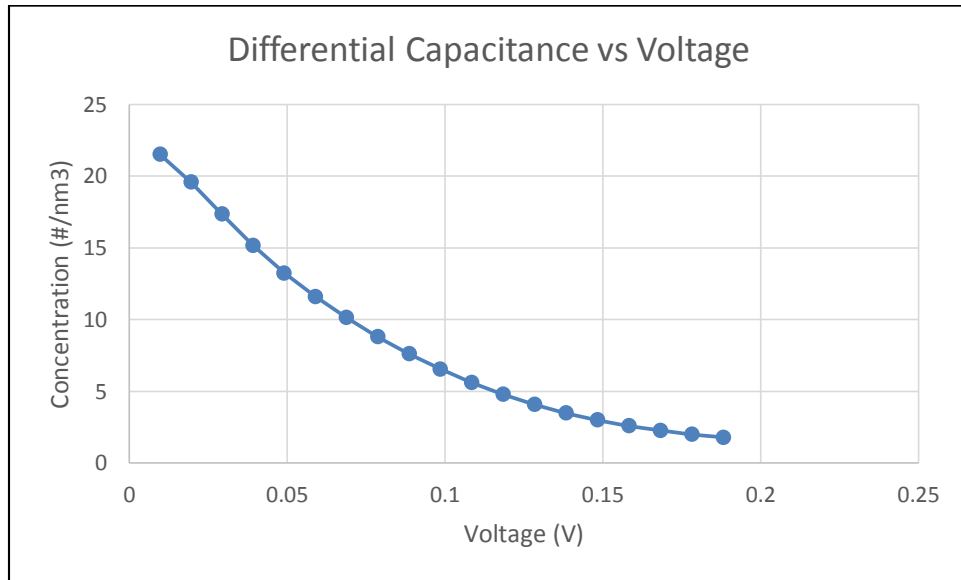
3.7.2 H_2SO_4 as electrolyte

Figure 3.10: Differential Capacitance vs Positive Voltage (0.2V)

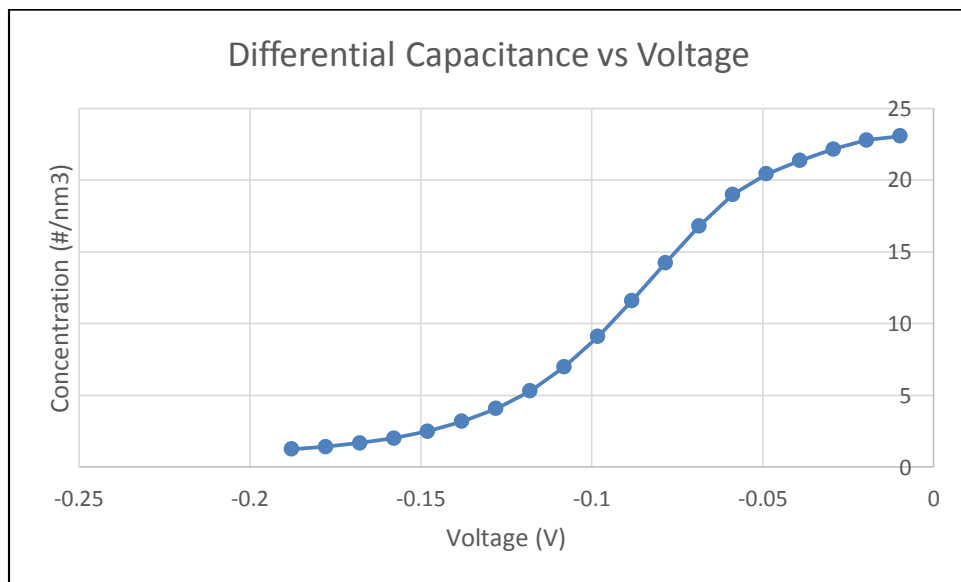Given below is the plot for negative voltage.

Figure 3.11: Differential Capacitance vs Negative Voltage (0.2V)

Graphs for both cases (positive and negative voltage) and both electrolytes need to be combined for our study. We shall study this curve in detail in next section.

Chapter 4

RESULTS AND DISCUSSION

In this chapter, we obtain the results and study various parameters such as Packing fraction, velocity, electrical displacement, etc. A voltage of 0.2V was applied in case of both electrolytes and the temperatures were varied from 298K to 313K and then to 333.

4.1 KOH as electrolyte

4.1.1 Positive Voltage applied at room temperature

Following plots were obtained for various parameters.
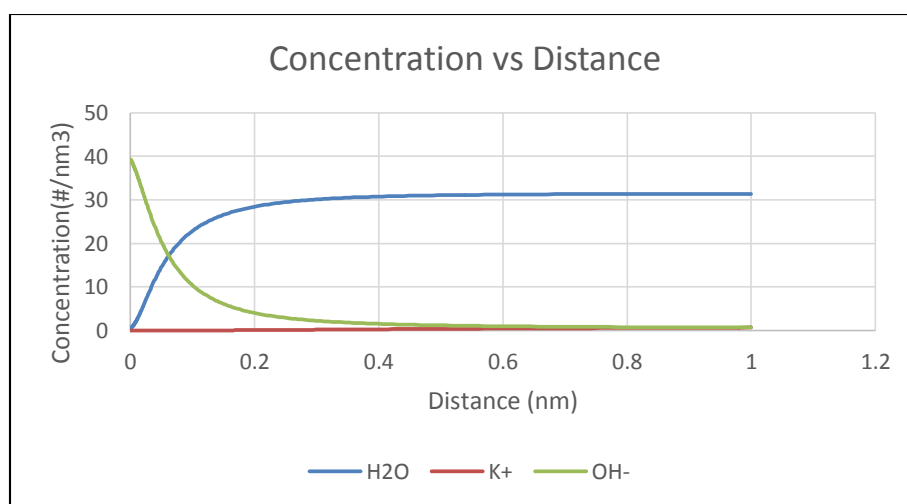
4.1.1.1 Concentration

Figure 4.1: Concentration vs Distance at 298K for KOH

As it can be seen in the graph above, upon the application of positive voltage, anions get accumulated near the electrode by displacing water particles.

There is a slight increase in concentration of potassium (cations) away from the electrode.

4.1.1.2 Packing Fraction

This parameter is analogous to the concentration of counterions near the electrode surface. Hence, dense accumulation leads to higher packing fraction value. As, the distance from electrode approaches the Debye length, the value starts decreasing and then remains constant, similar to that of concentration. The plot is shown below.
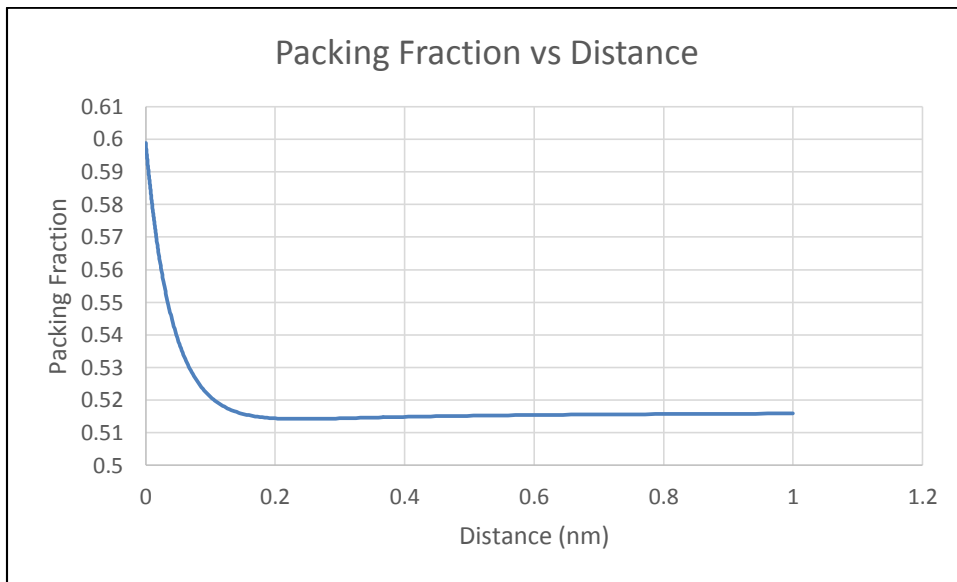

Figure 4.2: Packing Fraction vs Distance at 298K for KOH

4.1.1.3 Velocity

There is always some voltage present just outside the double layer. This voltage causes ions in the diffuse part causing the ions to drag through the liquid and generates the velocity. It can be seen that packing fraction and velocity are

inversely related, meaning maximum velocity will be observed when the density is less. The plot for velocity is shown below.
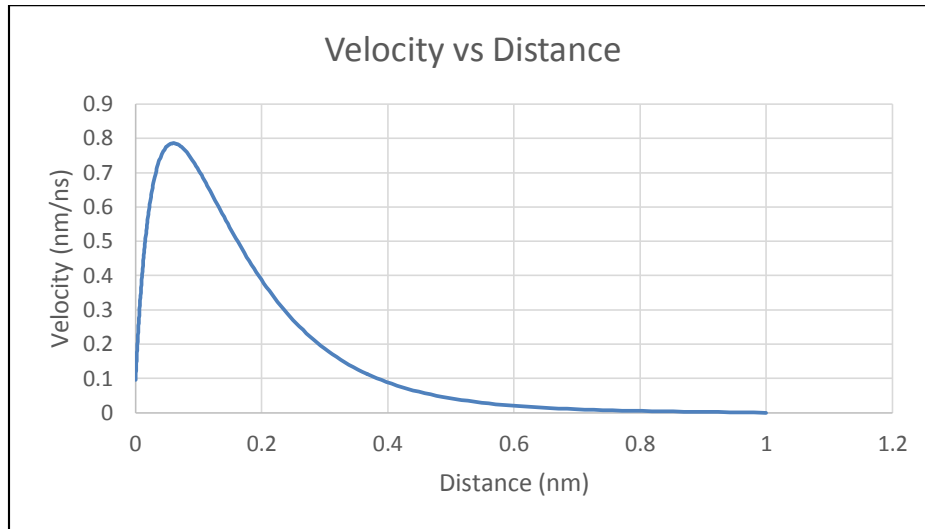

Figure 4.3: Velocity vs Distance at 298K for KOH

4.1.1.4 Electric Displacement

When electric potential is applied to a material, the charges that are bound to the surface start separating which induces a dipole moment. As seen in the plot below, it decreases steadily as we move away from electrode because potential decreases.
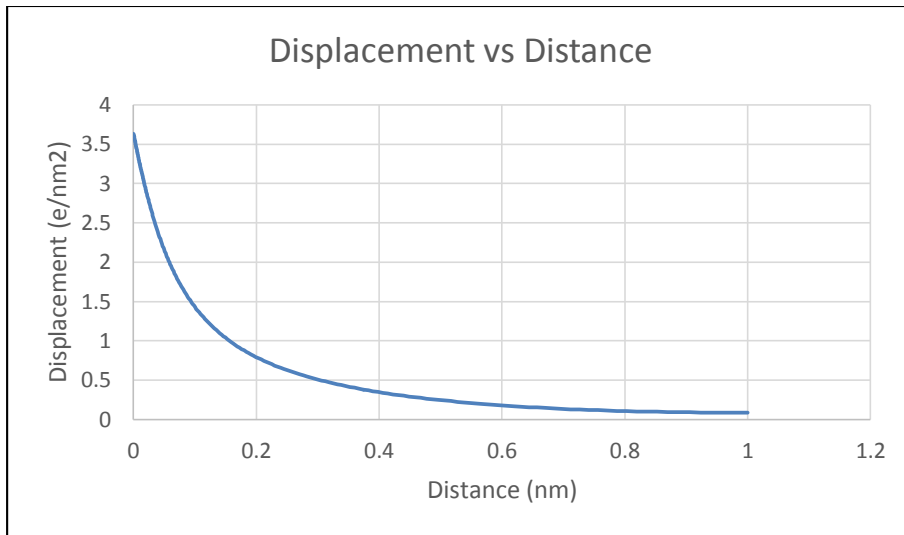
Figure 4.4: Displacement vs Distance at 298K for KOH

4.1.2 Temperature varied and Positive voltage applied

4.1.2.1 Packing Fraction
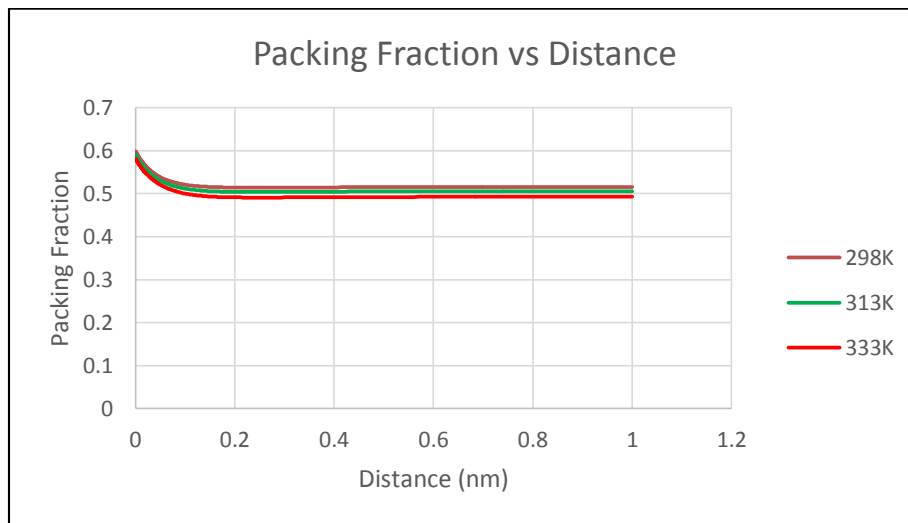
Figure 4.5: Packing Fraction vs Distance at various temperatures for KOH

Red line represents packing fraction at 333K while the orange line represents that at room temperature. It can be seen that packing fraction is highest

at lower temperature. This be due to the thermal motion of particles in the medium.

4.1.2.2 Velocity
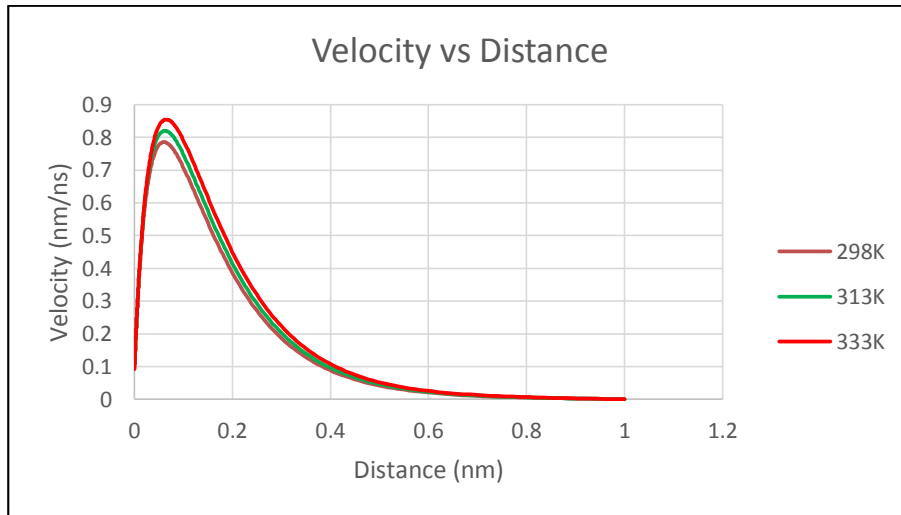
Figure 4.6: Velocity vs Distance at various temperatures for KOH

Velocity is highest at 333K, represented by red line and the least at 298K.

4.1.2.3 Electric Displacement
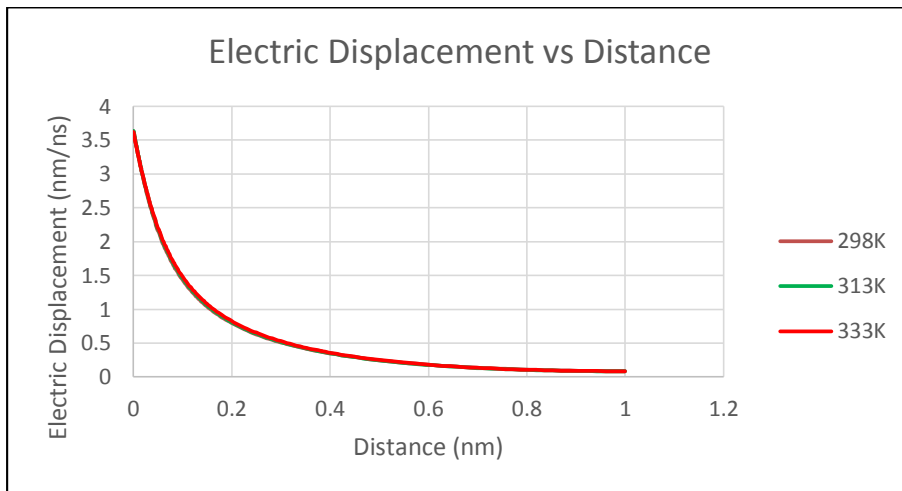
Figure 4.7: Electric Displacement vs Distance at various temperatures for KOH

As seen, displacement hardly changes along with change in temperature.

4.1.3 Negative Voltage applied at room temperature

4.1.3.1 Concentration
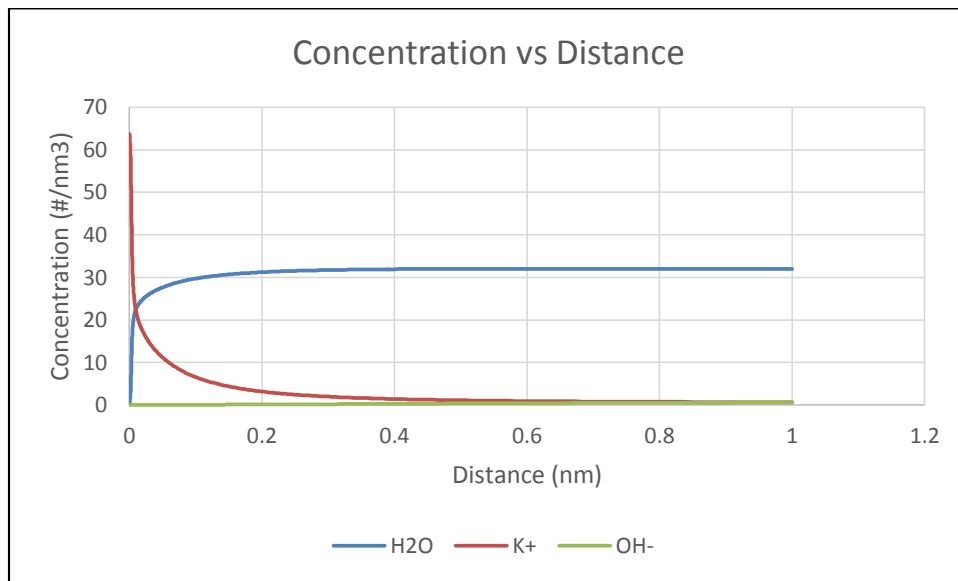
Figure 4.8: Concentration vs Distance at 298K for KOH (Negative Voltage)

Here it can be seen that positively charged potassium ions are concentrated near the electrode. Water particles have been displaced as seen in the previous case. Concentration of coions increases gradually. However, it is also observed that the concentration is very high as compared to the earlier case. Hence we can also observe that equilibrium is quickly attained as compared to previous case. Now let us study the effect on packing fraction.

4.1.3.2 Packing Fraction

The graph for packing fraction is more or less similar to the earlier case. The values are almost the same. However, as observed in case of concentration, packing fraction too remains constant after a very small length. It can also be seen that the value of this parameter is greater as compared to earlier case and hence density is observed to be high.
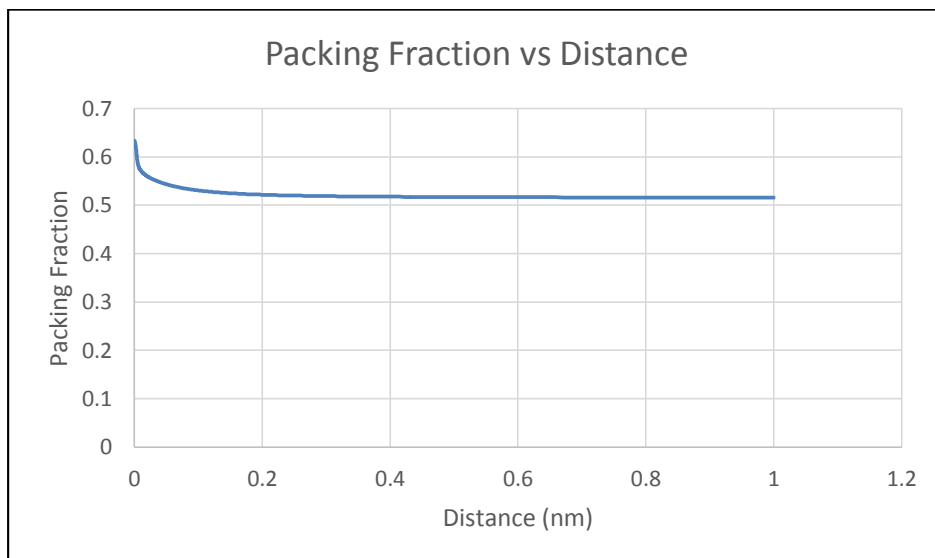
Figure 4.9: Packing Fraction vs Distance at 298K for KOH (Negative Voltage)

4.1.3.3 Velocity

It can be observed that the initial velocity is slightly high as compared to previous case. This corroborates our previous observations about concentration and packing fraction. However, an interesting observation here is that although, the initial velocity is on the higher side, the maximum velocity (0.35nm/ns) is far less than the earlier (0.78nm/ns).
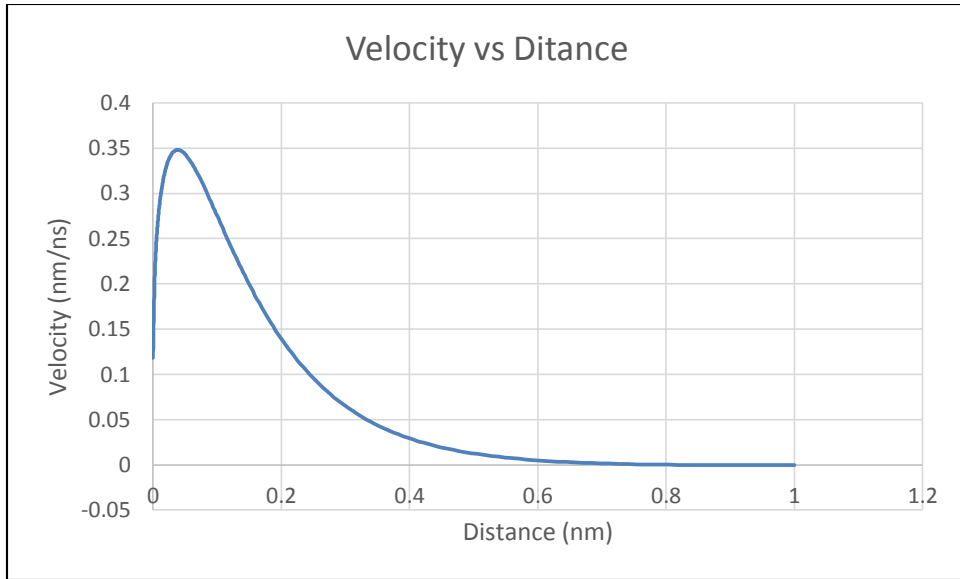
Figure 4.10: Velocity vs Distance at 298K for KOH (Negative Voltage)

4.1.3.4 Electric Displacement
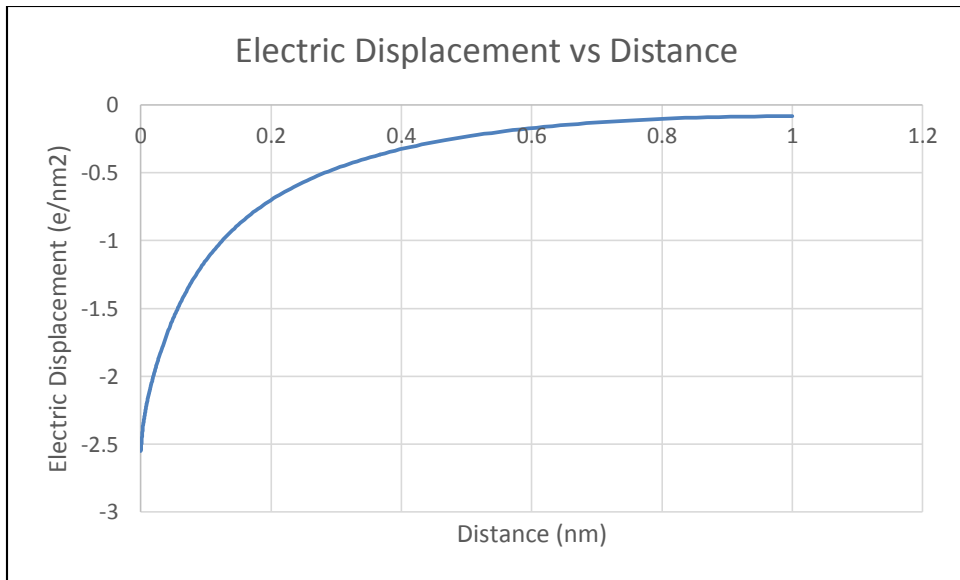
Figure 4.11: Electric Displacement vs Distance at 298K for KOH

(Negative Voltage)

Similar to the previous case, it decreases along the distance and potential.

4.1.4 Temperature varied and negative voltage applied

Procedure of varying the temperature was repeated as above and plots were obtained.

4.1.4.1 Packing Fraction:
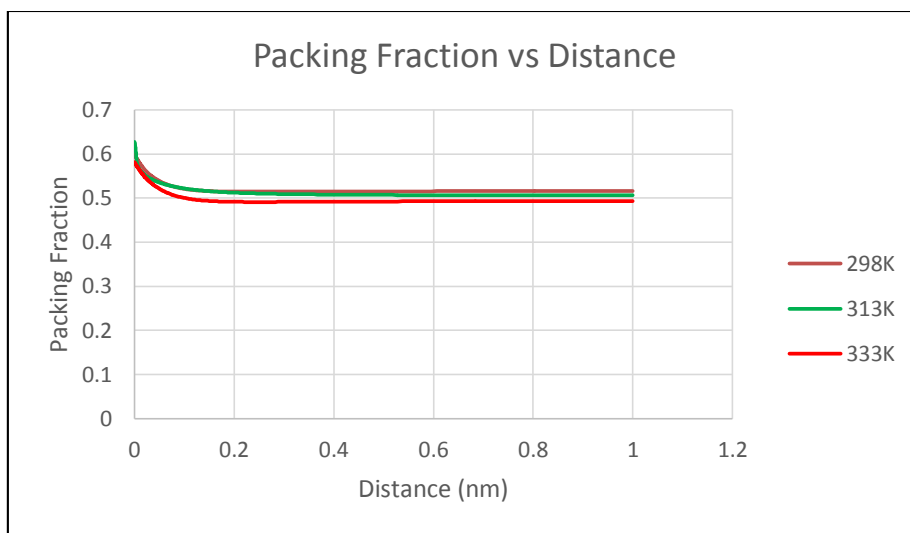
Figure 4.12: Packing Fraction vs Distance at varied temperatures for KOH

(Negative Voltage)

Packing fraction is least for highest temperature and highest at room temperature. This is exactly similar to previous case for positive voltage.

4.1.4.2 Velocity

Here, there is hardly any difference for velocities for 298K and 313K. However, there is a drastic change at 333K.
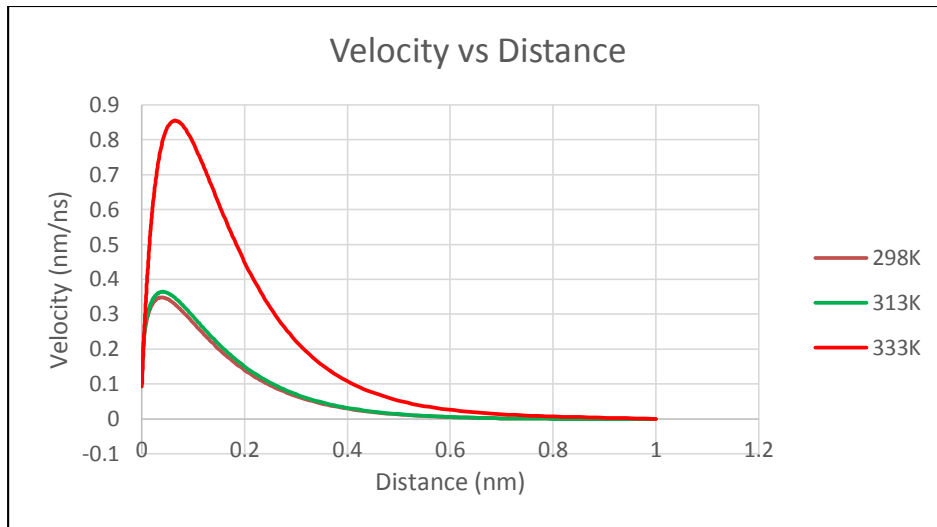
Figure 4.13: Velocity vs Distance at varied temperatures for KOH

(Negative Voltage)

4.1.4.3 Electric Displacement

It does not change with change in temperature.
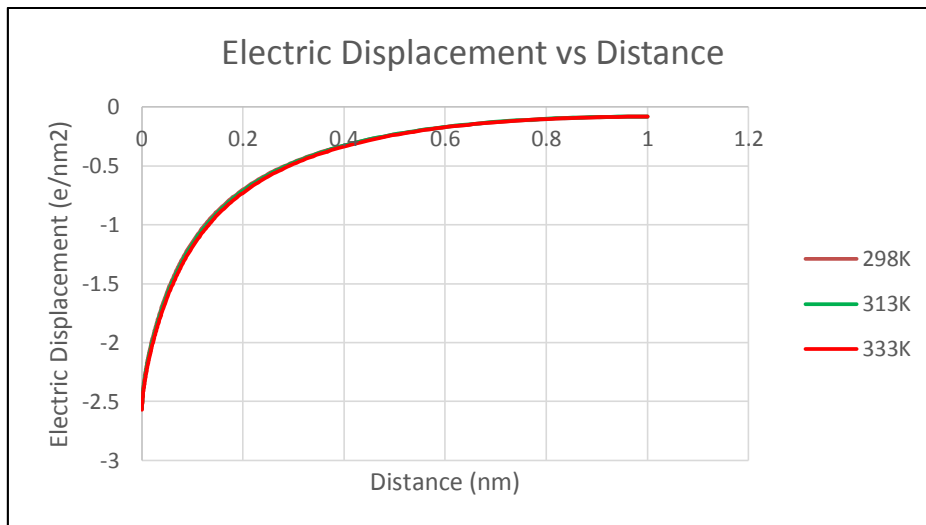
Figure 4.14: Electric Displacement vs Distance at varied temperatures for KOH

(Negative Voltage)

4.2 H_2SO_4 as electrolyte

4.2.1 Positive voltage applied at room temperature

4.2.1.1 Concentration
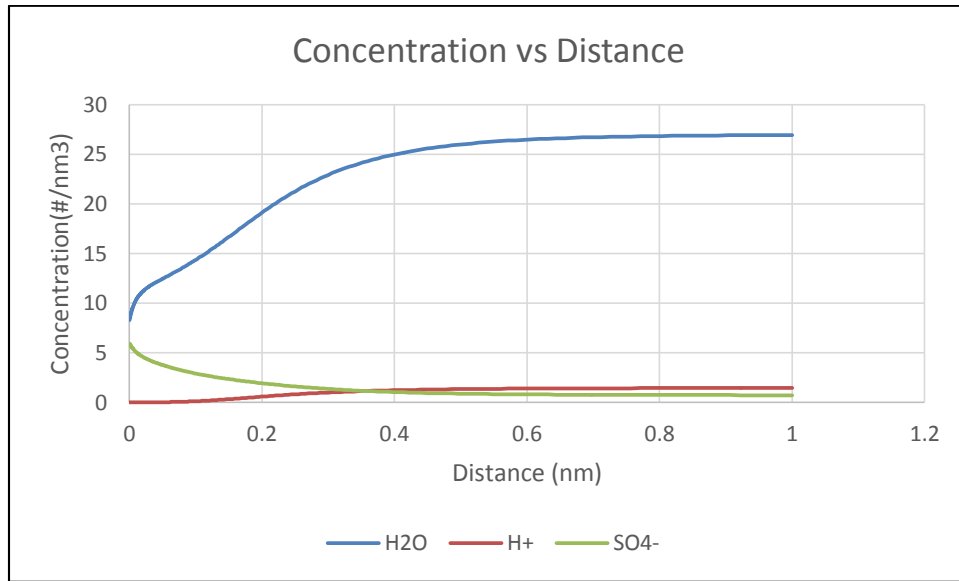
Figure 4.15: Concentration vs Distance at 298K for H_2SO_4

As seen, very high volume of water is displaced. Anions decrease gradually while the concentration of cations finally reaches a value greater than anions and stays constant.

4.2.1.2 Packing Fraction

For this electrolyte, initially a dip is observed followed by gradual rise and then it remains constant. This dip is in the region where the velocity is at its highest. This is not observed for KOH and neither was this observed for this electrolyte when negative voltage was applied. This happens due to cavitation phenomenon. Due to the applied voltage, cations are attracted towards the

electrode. If this happens very quickly, vacuum is formed creating a void or holes in the region, which momentarily decreases the pressure. Then, the particles from bulk start gaining the voids and thus pressure returns to normal and the packing fraction stabilizes. The plot below shows the drop in pressure.
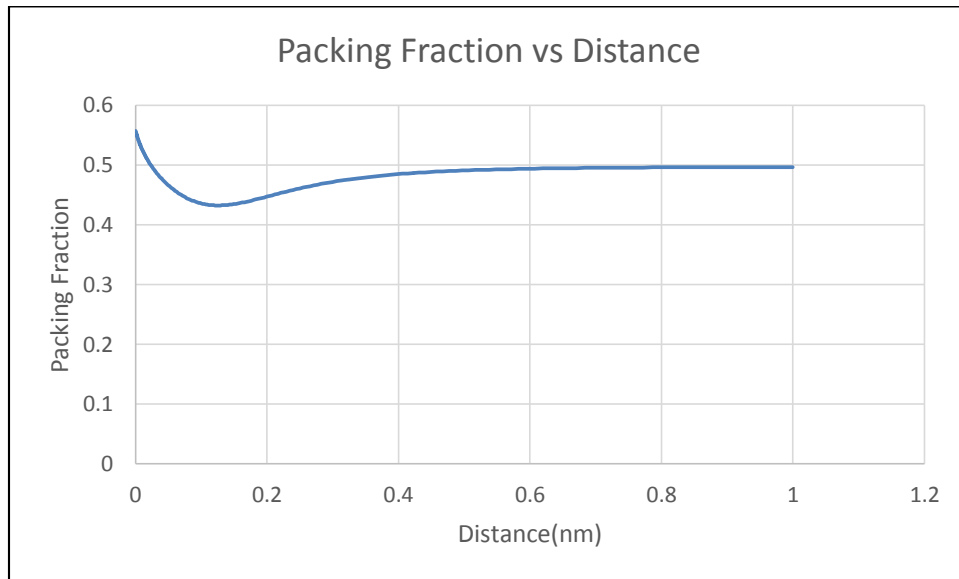
Figure 4.16: Packing Fraction vs Distance at 298K for H_2SO_4
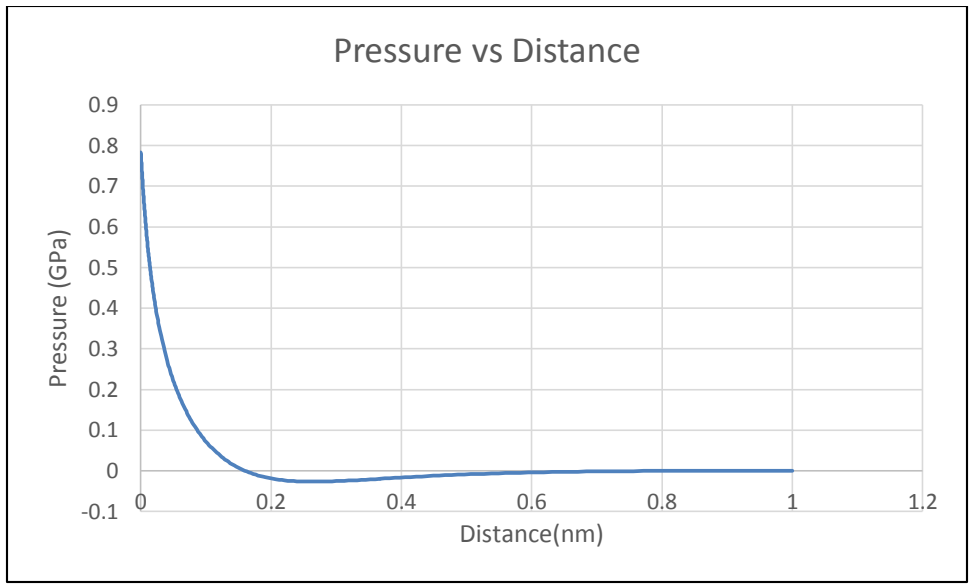
Figure 4.17: System Pressure vs Distance at 298K for H_2SO_4

4.2.1.3. Velocity
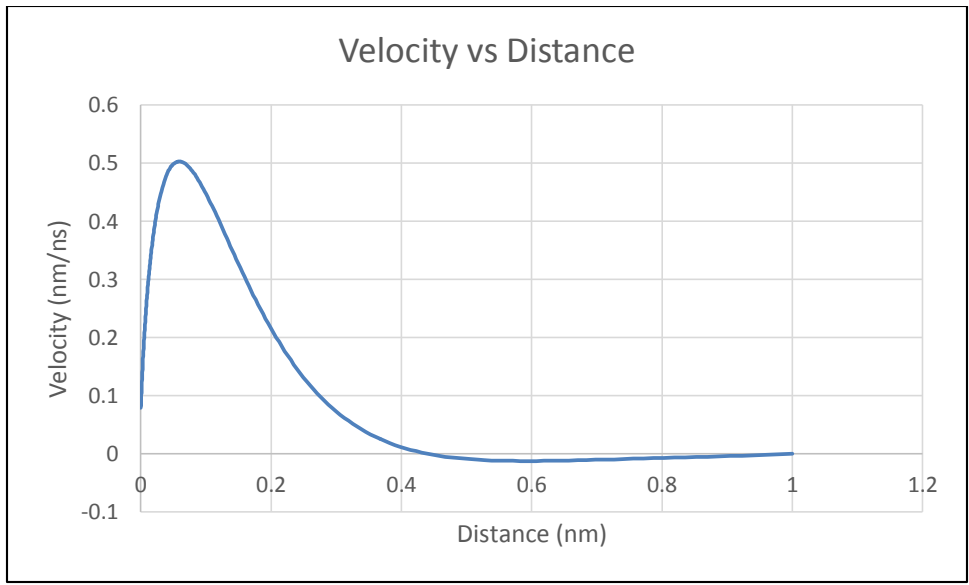
Figure 4.18: Velocity vs Distance at 298K for H_2SO_4

The plot is mostly similar to the previous ones, the only exception being it reaches a negative value before gradually increasing. This may be perhaps due to the increase in packing fraction. Velocity attains a constant value as that of packing fraction remains constant.

4.2.1.4 Electric Displacement
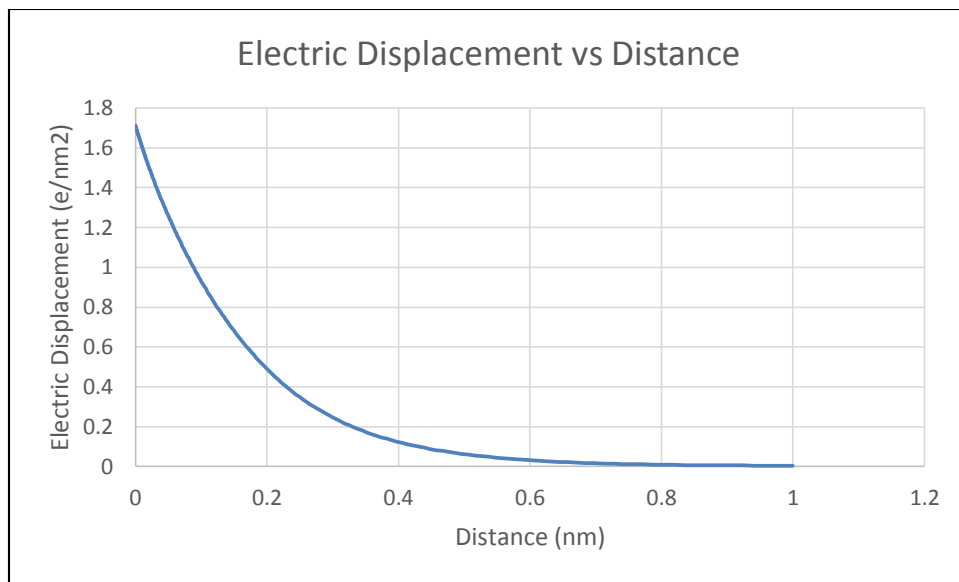
Figure 4.19: Electrical Displacement vs Distance at 298K for H_2SO_4

As in case of KOH, temperature is varied from room temperature to 313K and 333K. Packing fraction and velocity are the parameters that are considered and plots are obtained.

4.2.2 Temperature varied and positive voltage applied

4.2.2.1 Packing fraction

Packing fraction is the least at 333K and highest at 298K as observed and explained earlier.
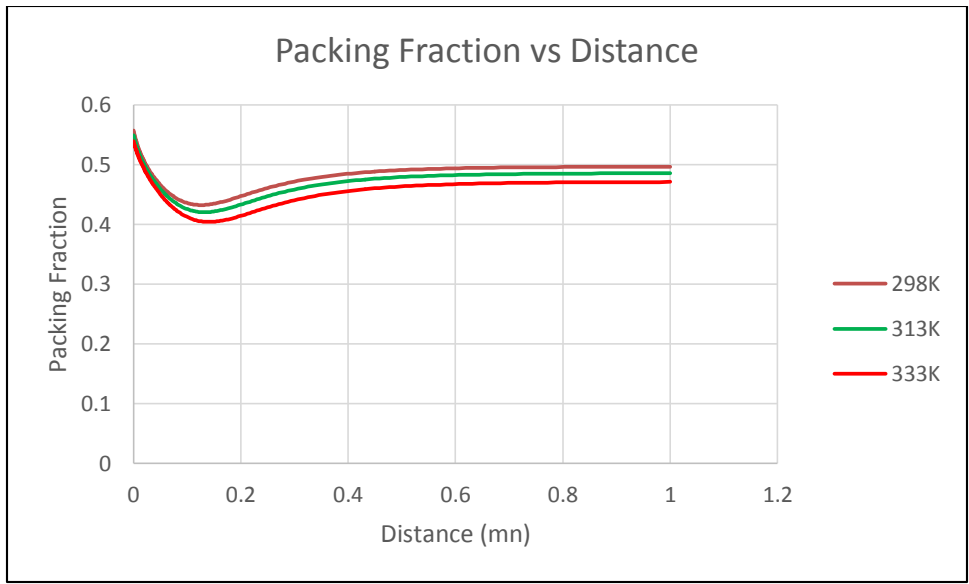
Figure 4.20: Packing Fraction vs Distance at varied temperature for H_2SO_4

4.2.2.2 Velocity
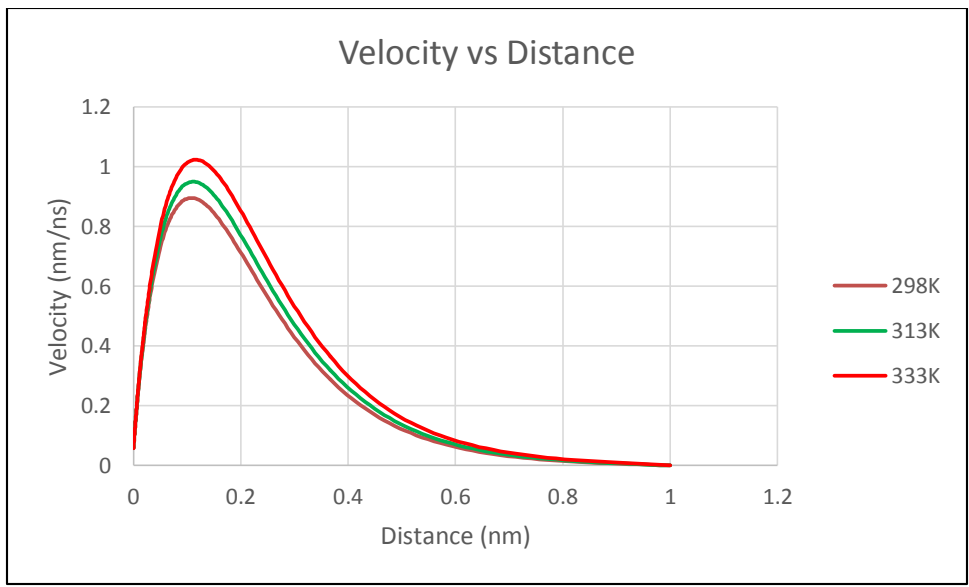
Figure 4.21: Velocity vs Distance at varied temperature for H_2SO_4

The plot shows that the velocity is highest at 333K (red line) and lowest at room temperature. This is in conjunction with our previous results.

4.2.2.3 Electrical Displacement
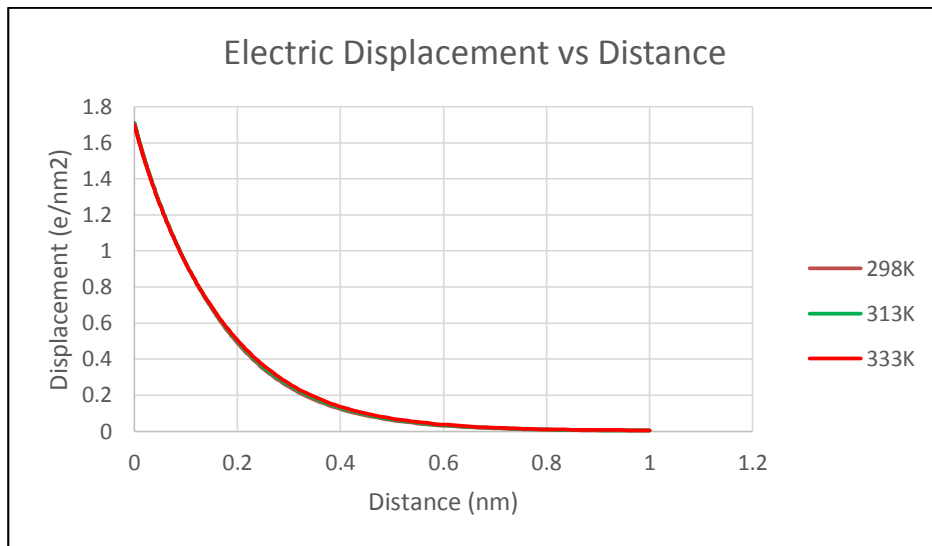
Figure 4.22: Electrical Displacement vs Distance at varied temperature for H_2SO_4

It hardly changes as per temperature, implying that it purely depends on electrical potential.

4.2.3. Negative voltage applied

Now plots are obtained when the applied voltage is negative and at room temperature.

4.2.3.1 Concentration

As negative voltage is applied, hydrogen ions can be seen concentrated towards electrode. They displace water particles. Concentration of sulphate ions keeps increasing.
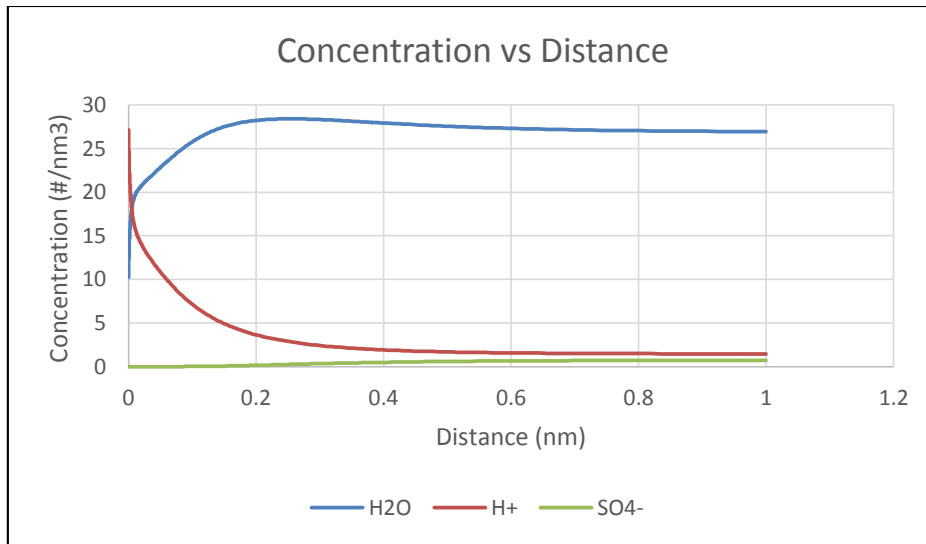
Figure 4.23: Concentration vs Distance at 298K for H_2SO_4 (Negative Voltage)

4.2.3.2 Packing Fraction
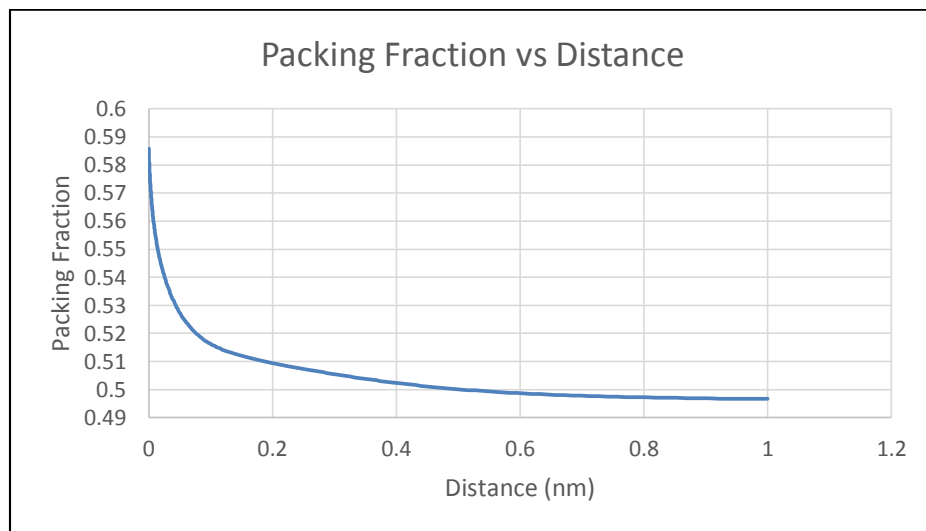
Figure 4.24: Concentration vs Distance at 298K for H_2SO_4 (Negative Voltage)

Packing fraction is highest near the electrode, decreases rapidly initially and then gradually.

4.2.3.3 Velocity
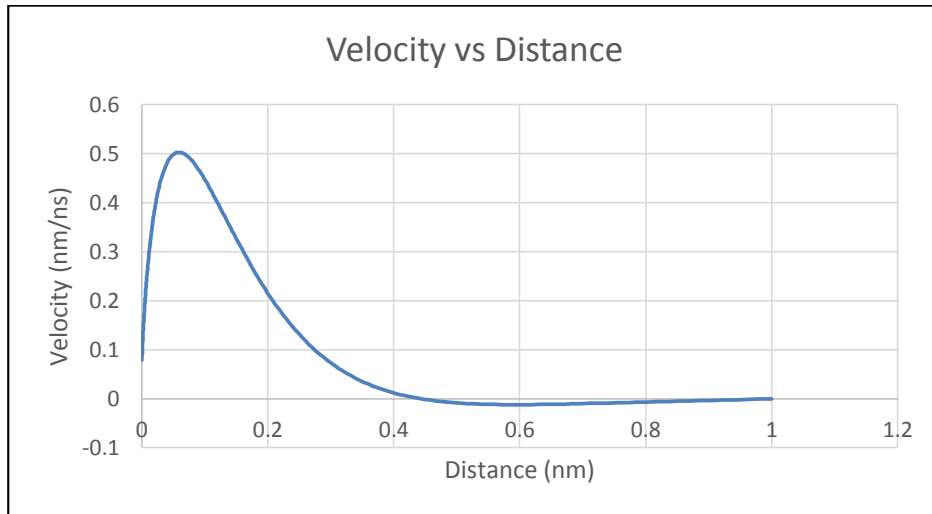
Figure 4.25: Velocity vs Distance at 298K for H_2SO_4 (Negative Voltage)

Velocity is highest in the region where the decrease in packing fraction is rapid. Here, decrease in velocity along with decrease in packing fraction is observed.

4.2.3.4 Electrical Displacement
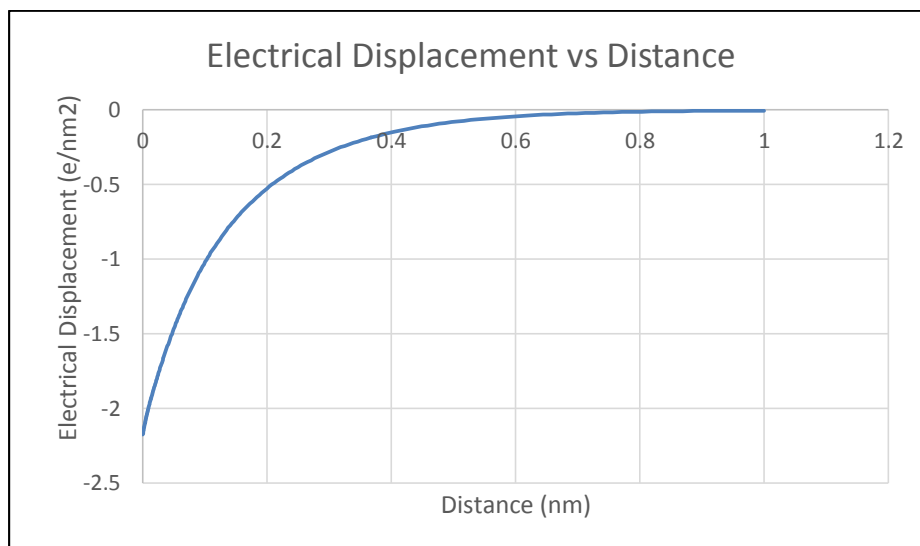
Figure 4.26: Displacement vs Distance at 298K for H_2SO_4 (Negative Voltage)

The plot shown above is exactly similar to the previous ones and hence, the same inferences.

4.2.4 Temperature varied and negative voltage applied

4.2.4.1 Packing Fraction
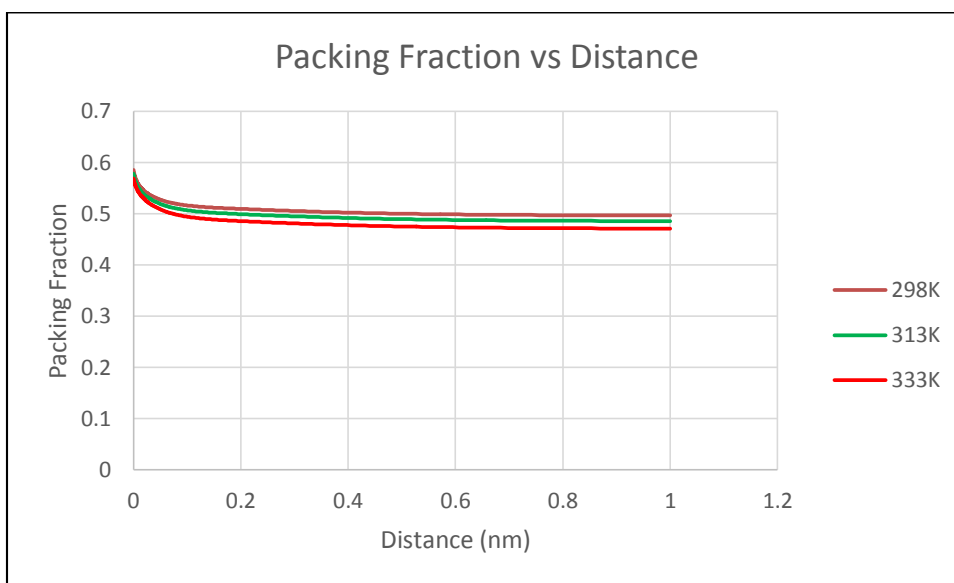
Figure 4.27: Packing Fraction vs Distance at varied temperature for H_2SO_4

(Negative Voltage)

Packing fraction is the least at 333K and highest at 298K as observed and explained earlier.

4.2.4.2 Velocity

The plot shown below that the velocity is highest at 333K (red line) and lowest at room temperature. This is in conjunction with our previous results.
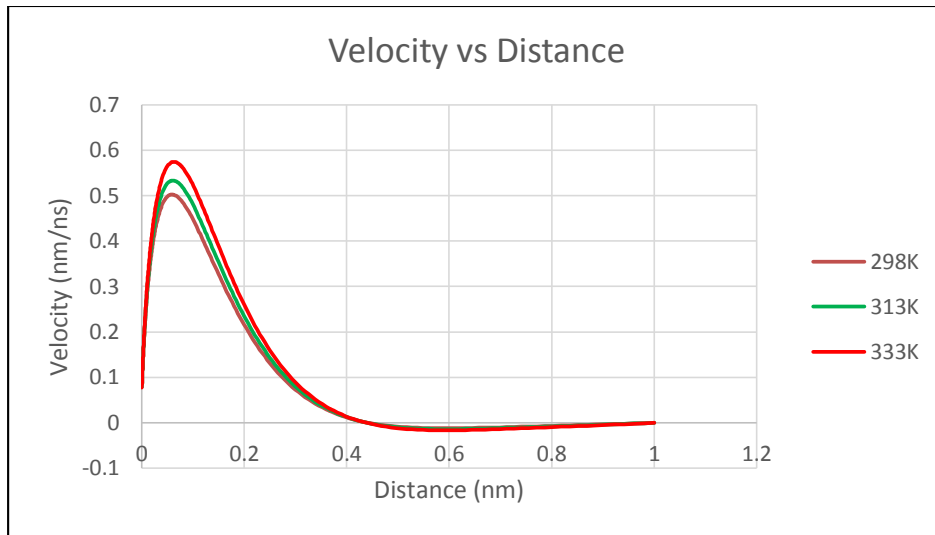
Figure 4.28: Velocity vs Distance at varied temperature for H_2SO_4

(Negative Voltage)

4.2.4.3 Electrical Displacement
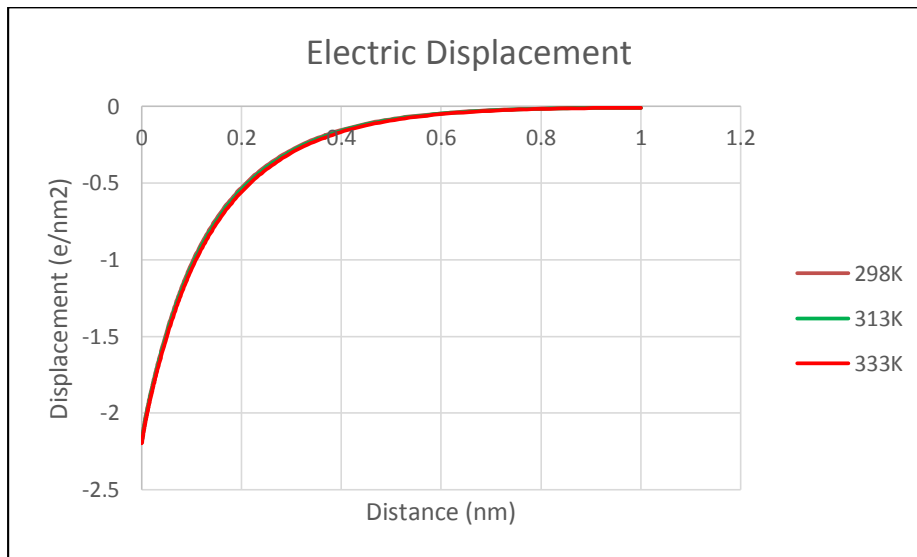
Figure 4.29: Electric Displacement vs Distance at varied temperature for H_2SO_4

(Negative Voltage)

Electric displacement does not change much with temperature as seen above.

## 4.3 Differential Capacitance

4.3.1 KOH as electrolyte
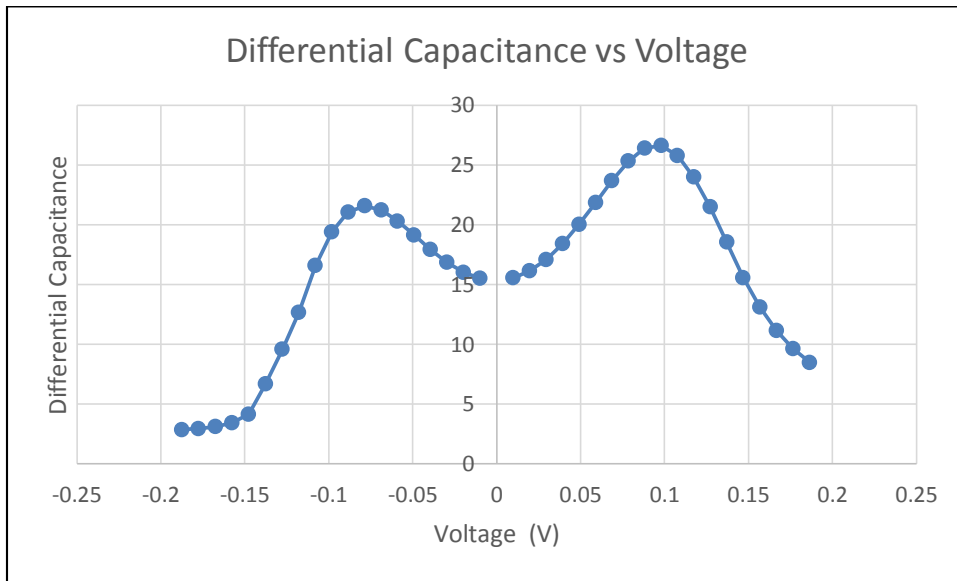
Figure 4.30: Differential Capacitance vs Voltage at 298K for KOH

We obtain a camel-shaped curve of differential capacitance over the voltage. We can clearly see that the curve is not perfectly symmetric. This is due to the difference size of ions (cations and anions). The characteristic 'U' shape is formed due to continuous condensation of ions on the electrode surface. This should ideally continue infinitely as shown in the diagram shown below. The dotted line shows rise in capacitance up to infinity, as predicted by Gouy Chapman and Poisson Boltzmann model. But due to saturation, condensation stops giving rise to a hump.
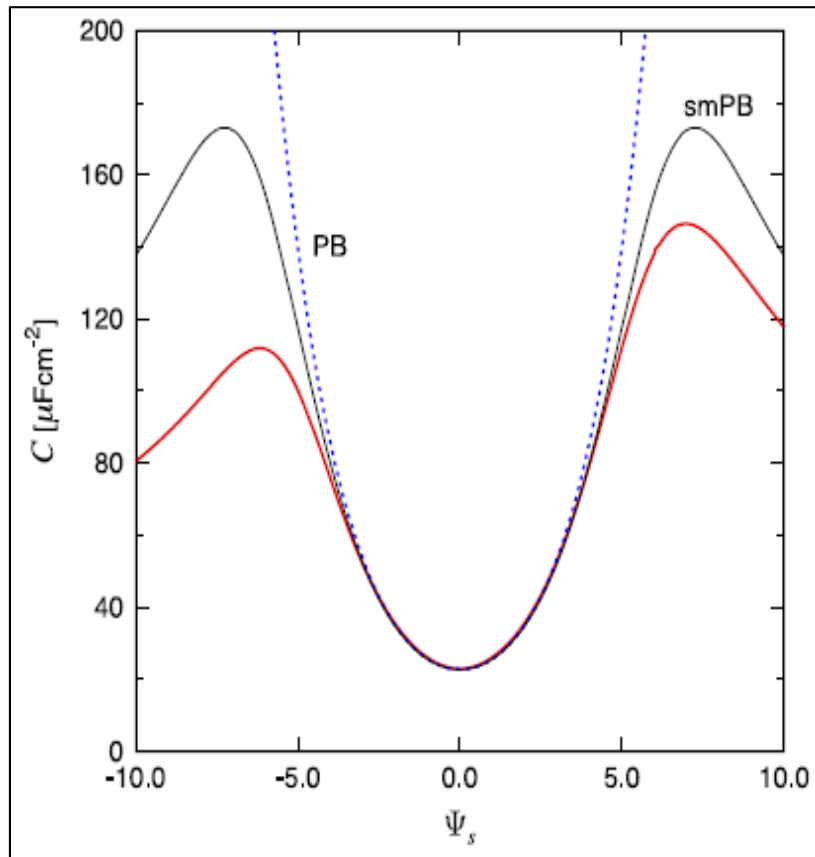
Figure 4.31: Concentration vs Distance at 298K for H_2SO_4 [26]

The saturation is caused due to size of ions termed as 'Steric' phenomenon.

A slight drop in differential capacitance was seen as temperature was varied. The

grey colored line represents the value at 298K while the red line represents 333K.
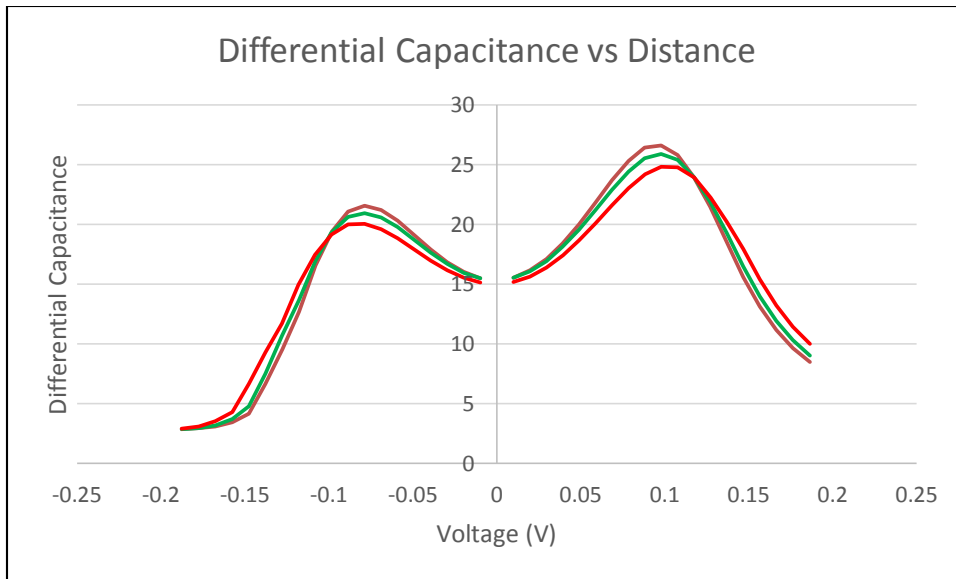
Figure 4.32: Differential Capacitance vs Voltage at varied temperature for KOH

The 'U' shape becomes increasingly broad as temperature rises.

4.3.2 H2SO4 as electrolyte
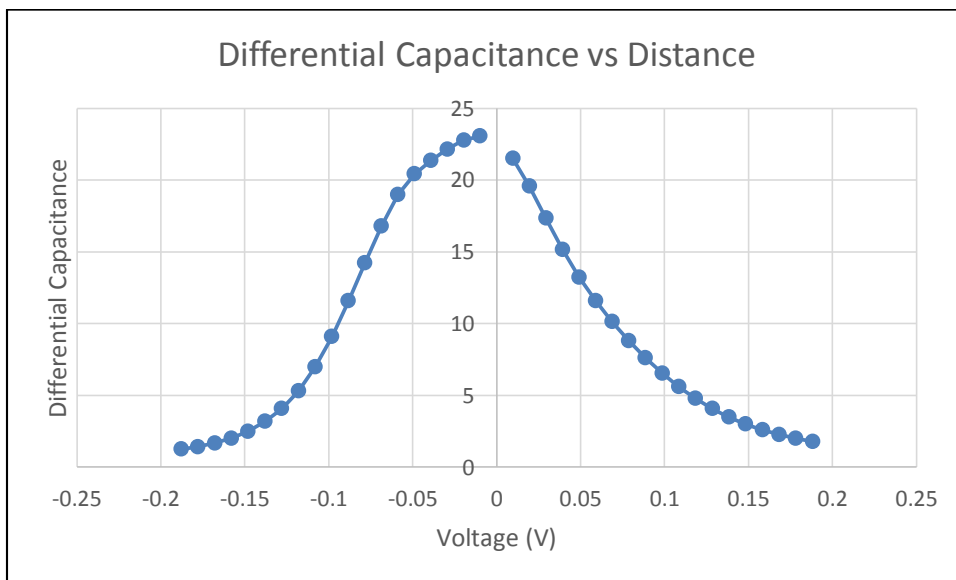
Figure 4.33: Differential Capacitance vs Voltage at 298K for H_2SO_4

The curve obtained for this electrolyte is entirely different from that of KOH. There is no camel shaped curve. This type of curve has been observed for solutions with high concentration of salts. Here, highest capacitance is seen at zero voltage.
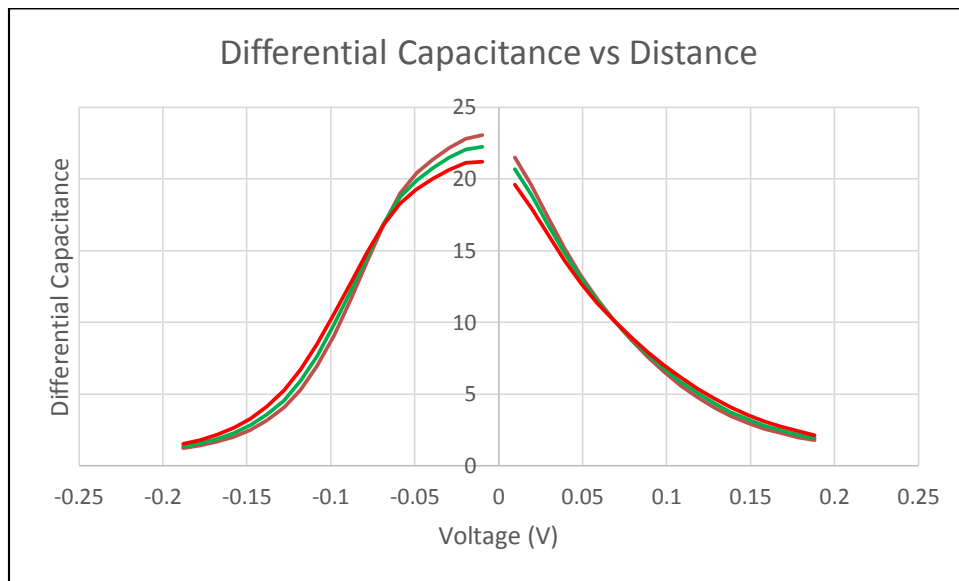
Figure 4.34: Differential Capacitance vs Voltage at varied temperature for H_2SO_4

Decrease in capacitance with rise in temperature is seen. Lowermost line is for 333K and highest for 298K with 313K in the middle.

Chapter 5

Conclusions

- A parametric study of two different electrolyte systems for a supercapacitor has been carried out. The theory we apply is capable of capturing the electrolyte saturation effect at the electrode surface and dealing with multicomponent electrolytes.

- Relationship between Differential Capacitance and Double Layer structure has been studied and following inferences deduced:

  - ✓ The two electrolyte systems studied exhibit characteristically different behaviors.

  - ✓ The camel shape of the differential capacitance curve should be due to the counterion saturation effect at the electrode surface.

  - ✓ The asymmetric differential capacitance curve should be due to the different properties of counterions when the voltage is positive or negative.

Appendix

Input Profile

1. Input Profile for 298K

```
************1D Problem*******************
1               !=1 if planar; =2 if cylindrical; =3 if spherical
298             !Temperature(K)
************Domain and Grid*****************
0, 1, 250, 1.02 !XStt,XEnd(nm),Total # of divisions,Mesh-grading power
************Involved Chemical Components*********
3       !Total#Of Involved Chemical Components
1, 2, 3         !Above#X(ID_Glb of Involved Chemical Component)
************Involved Chemical Reactions*********
0       !Total#Of Involved Chemical Reactions
        !Above#X(ID_Glb Of Involved Chemical Reaction)
*************Simulation Time & Steps*******************
20, 20          !NtotTimeSteps,NtotSnapShots
0               !ITimeStt(=0, first time run; >0, to restart based on ITimeStt-1 step)
************Initial Uniform Concentrations*******************
31.97, 0.6144, 0.6144    !C(particle/nm^3)///MUST Follow the above order of involved chemical components
*************Boundary Condition*************
!---repeat below !NthC,Ramp1Jump2,2(Flux0_End,SpringCoef_End,C_Eqilibrium_End)
0, 1, 0, 1.d3, 0.2, 0, 1.d3, 0 !electric (Displacement=Displacement0+Coef*(V-V0)) with displacement_unit:e/nm^2
1, 2, 0, 0, 0, 0, 1.d3, 31.97   !chemical (flux=flux0+Coef*(C-C0)) with flux_unit:particle/nm^2/ns, and C_unit:particle/nm^3
2, 2, 0, 0, 0, 0, 1.d3, 0.6144  !chemical (flux=flux0+Coef*(C-C0)) with flux_unit:particle/nm^2/ns, and C_unit:particle/nm^3
3, 2, 0, 0, 0, 0, 1.d3, 0.6144  !chemical (flux=flux0+Coef*(C-C0)) with flux_unit:particle/nm^2/ns, and C_unit:particle/nm^3
*************Numerical Parameters*******************
90000, 1.d-3, 1000, 0.002       !IteratMax,ErrAllow,IteratDisplay,ARelax
*******************************************************
************All Chemical Components*******************
3       !Total # of chemical components
--repeat (above #) below--!ID;Valance;Relative_Permittivity@Linear;StokesRadius;PhysicalRadius;EtaOverEpsil0((V/nm)^2-nS);Avdw0
1,  0,   79, 0.09687,   0.1552, 0.113d1, 0.20294       !H2O(0)(10)
2,  1,   5.55, 0.125,     0.133, 0.113d1, 0.20294       !K(1+)(39)
3, -1,   64.4, 0.0431,    0.153, 0.113d1, 0.20294       !OH(1-)(17)
```

```
************1D Problem*******************
1               !=1 if planar; =2 if cylindrical; =3 if spherical
298             !Temperature(K)
************Domain and Grid*****************
0, 1, 250, 1.02 !XStt,XEnd(nm),Total # of divisions,Mesh-grading power
************Involved Chemical Components*********
3       !Total#Of Involved Chemical Components
1, 2, 3         !Above#X(ID_Glb of Involved Chemical Component)
************Involved Chemical Reactions*********
0       !Total#Of Involved Chemical Reactions
        !Above#X(ID_Glb Of Involved Chemical Reaction)
*************Simulation Time & Steps*******************
20, 20          !NtotTimeSteps,NtotSnapShots
0               !ITimeStt(=0, first time run; >0, to restart based on ITimeStt-1 step)
************Initial Uniform Concentrations*******************
31.97, 0.6144, 0.6144    !C(particle/nm^3)///MUST Follow the above order of involved chemical components
*************Boundary Condition*************
!---repeat below !NthC,Ramp1Jump2,2(Flux0_End,SpringCoef_End,C_Eqilibrium_End)
0, 1, 0, 1.d3, -0.2, 0, 1.d3, 0 !electric (Displacement=Displacement0+Coef*(V-V0)) with displacement_unit:e/nm^2
1, 2, 0, 0, 0, 0, 1.d3, 31.97   !chemical (flux=flux0+Coef*(C-C0)) with flux_unit:particle/nm^2/ns, and C_unit:particle/nm^3
2, 2, 0, 0, 0, 0, 1.d3, 0.6144  !chemical (flux=flux0+Coef*(C-C0)) with flux_unit:particle/nm^2/ns, and C_unit:particle/nm^3
3, 2, 0, 0, 0, 0, 1.d3, 0.6144  !chemical (flux=flux0+Coef*(C-C0)) with flux_unit:particle/nm^2/ns, and C_unit:particle/nm^3
*************Numerical Parameters*******************
90000, 1.d-3, 1000, 0.002       !IteratMax,ErrAllow,IteratDisplay,ARelax
*******************************************************
************All Chemical Components*******************
3       !Total # of chemical components
--repeat (above #) below--!ID;Valance;Relative_Permittivity@Linear;StokesRadius;PhysicalRadius;EtaOverEpsil0((V/nm)^2-nS);Avdw0
1,  0,   79, 0.09687,   0.1552, 0.113d1, 0.20294       !H2O(0)(10)
2,  1,   5.55, 0.125,     0.133, 0.113d1, 0.20294       !K(1+)(39)
3, -1,   64.4, 0.0431,    0.153, 0.113d1, 0.20294       !OH(1-)(17)
```

2. Input Profile for 313K

```
************1D Problem******************
1               !=1 if planar; =2 if cylindrical; =3 if spherical
313             !Temperature(K)
************Domain and Grid******************
0, 1, 250, 1.02 !XStt,XEnd(nm),Total # of divisions,Mesh-grading power
************Involved Chemical Components*********
3       !Total#Of Involved Chemical Components
1, 2, 3         !Above#X(ID_Glb Of Involved Chemical Component)
************Involved Chemical Reactions*********
0       !Total#Of Involved Chemical Reactions
        !Above#X(ID_Glb Of Involved Chemical Reaction)
************Simulation Time & Steps******************
20, 20          !NtotTimeSteps,NtotSnapShots
0               !ITimeStt(=0, first time run; >0, to restart based on ITimeStt-1 step)
************Initial Uniform Concentrations******************
31.255, 0.6675, 0.6675     !C(particle/nm^3)///MUST Follow the above order of involved chemical components
************Boundary Condition*************
!---repeat below !NthC,Ramp1Jump2,2(Flux0_End,SpringCoef_End,C_Eqilibrium_End)
0, 1, 0, 1.d3, 0.2, 0, 1.d3, 0  !electric (Displacement=Displacement0+Coef*(V-V0)) with displacement_unit:e/nm^2
1, 2, 0, 0, 0, 0, 1.d3, 31.255  !chemical (flux=flux0+Coef*(C-C0)) with flux_unit:particle/nm^2/ns, and C_unit:particle/nm^3
2, 2, 0, 0, 0, 0, 1.d3, 0.6675  !chemical (flux=flux0+Coef*(C-C0)) with flux_unit:particle/nm^2/ns, and C_unit:particle/nm^3
3, 2, 0, 0, 0, 0, 1.d3, 0.6675  !chemical (flux=flux0+Coef*(C-C0)) with flux_unit:particle/nm^2/ns, and C_unit:particle/nm^3
************Numerical Parameters******************
90000, 1.d-3, 1000, 0.002       !IteratMax,ErrAllow,IteratDisplay,ARelax
******************************************************
************All Chemical Components******************
3       !Total # of chemical components
--repeat (above #) below--!ID;Valance;Relative_Permittivity@Linear;StokesRadius;PhysicalRadius;EtaOverEpsil0((V/nm)^2-nS);Avdw0
1,  0,   79, 0.09687,   0.1552, 0.113d1, 0.20294       !H2O(0)(10)
2,  1,  5.55,  0.125,    0.133, 0.113d1, 0.20294       !K(1+)(39)
3, -1,   64.4,  0.0431,    0.153, 0.113d1, 0.20294      !OH(1-)(17)
```

```
************1D Problem******************
1               !=1 if planar; =2 if cylindrical; =3 if spherical
313             !Temperature(K)
************Domain and Grid******************
0, 1, 250, 1.02 !XStt,XEnd(nm),Total # of divisions,Mesh-grading power
************Involved Chemical Components*********
3       !Total#Of Involved Chemical Components
1, 2, 3         !Above#X(ID_Glb Of Involved Chemical Component)
************Involved Chemical Reactions*********
0       !Total#Of Involved Chemical Reactions
        !Above#X(ID_Glb Of Involved Chemical Reaction)
************Simulation Time & Steps******************
20, 20          !NtotTimeSteps,NtotSnapShots
0               !ITimeStt(=0, first time run; >0, to restart based on ITimeStt-1 step)
************Initial Uniform Concentrations******************
31.255, 0.6675, 0.6675     !C(particle/nm^3)///MUST Follow the above order of involved chemical components
************Boundary Condition*************
!---repeat below !NthC,Ramp1Jump2,2(Flux0_End,SpringCoef_End,C_Eqilibrium_End)
0, 1, 0, 1.d3, -0.2, 0, 1.d3, 0 !electric (Displacement=Displacement0+Coef*(V-V0)) with displacement_unit:e/nm^2
1, 2, 0, 0, 0, 0, 1.d3, 31.255  !chemical (flux=flux0+Coef*(C-C0)) with flux_unit:particle/nm^2/ns, and C_unit:particle/nm^3
2, 2, 0, 0, 0, 0, 1.d3, 0.6675  !chemical (flux=flux0+Coef*(C-C0)) with flux_unit:particle/nm^2/ns, and C_unit:particle/nm^3
3, 2, 0, 0, 0, 0, 1.d3, 0.6675  !chemical (flux=flux0+Coef*(C-C0)) with flux_unit:particle/nm^2/ns, and C_unit:particle/nm^3
************Numerical Parameters******************
90000, 1.d-3, 1000, 0.002       !IteratMax,ErrAllow,IteratDisplay,ARelax
******************************************************
************All Chemical Components******************
3       !Total # of chemical components
--repeat (above #) below--!ID;Valance;Relative_Permittivity@Linear;StokesRadius;PhysicalRadius;EtaOverEpsil0((V/nm)^2-nS);Avdw0
1,  0,   79, 0.09687,   0.1552, 0.113d1, 0.20294       !H2O(0)(10)
2,  1,  5.55,  0.125,    0.133, 0.113d1, 0.20294       !K(1+)(39)
3, -1,   64.4,  0.0431,    0.153, 0.113d1, 0.20294      !OH(1-)(17)
```

3. Input Profile for 333K

```
************1D Problem******************
1                !=1 if planar; =2 if cylindrical; =3 if spherical
333              !Temperature(K)
************Domain and Grid******************
0, 1, 250, 1.02 !XStt,XEnd(nm),Total # of divisions,Mesh-grading power
************Involved Chemical Components*********
3        !Total#Of Involved Chemical Components
1, 2, 3          !Above#X(ID_Glb of Involved Chemical Component)
************Involved Chemical Reactions*********
0        !Total#Of Involved Chemical Reactions
         !Above#X(ID_Glb Of Involved Chemical Reaction)
************Simulation Time & Steps******************
20, 20           !NtotTimeSteps,NtotSnapShots
0                !ITimeStt(=0, first time run; >0, to restart based on ITimeStt-1 step)
************Initial Uniform Concentrations******************
30.3865, 0.7, 0.7         !C(particle/nm^3)///MUST Follow the above order of involved chemical components
************Boundary Condition************
!---repeat below !NthC,Ramp1Jump2,2(Flux0_End,SpringCoef_End,C_Eqilibrium_End)|
0, 1, 0, 1.d3, 0.2, 0, 1.d3, 0  !electric (Displacement=Displacement0+Coef*(V-V0)) with displacement_unit:e/nm^2
1, 2, 0, 0, 0, 0, 1.d3, 30.3865 !chemical (flux=flux0+Coef*(C-C0)) with flux_unit:particle/nm^2/ns, and C_unit:particle/nm^3
2, 2, 0, 0, 0, 0, 1.d3, 0.7      !chemical (flux=flux0+Coef*(C-C0)) with flux_unit:particle/nm^2/ns, and C_unit:particle/nm^3
3, 2, 0, 0, 0, 0, 1.d3, 0.7      !chemical (flux=flux0+Coef*(C-C0)) with flux_unit:particle/nm^2/ns, and C_unit:particle/nm^3
************Numerical Parameters******************
90000, 1.d-3, 1000, 0.002        !IteratMax,ErrAllow,IteratDisplay,ARelax
**********************************************************
************All Chemical Components******************
3        !Total # of chemical components
--repeat (above #) below--!ID;Valance;Relative_Permittivity@Linear;StokesRadius;PhysicalRadius;EtaOverEpsil0((V/nm)^2-ns);AvdW0
 1,  0,   79, 0.09687,   0.1552,  0.113d1, 0.20294       !H2o(0)(10)
 2,  1,   5.55, 0.125,   0.133,   0.113d1, 0.20294       !K(1+)(39)
 3, -1,   64.4,  0.0431,   0.153,  0.113d1, 0.20294       !OH(1-)(17)
```

```
************1D Problem******************
1                !=1 if planar; =2 if cylindrical; =3 if spherical
333              !Temperature(K)
************Domain and Grid******************
0, 1, 250, 1.02 !XStt,XEnd(nm),Total # of divisions,Mesh-grading power
************Involved Chemical Components*********
3        !Total#Of Involved Chemical Components
1, 2, 3          !Above#X(ID_Glb of Involved Chemical Component)
************Involved Chemical Reactions*********
0        !Total#Of Involved Chemical Reactions
         !Above#X(ID_Glb Of Involved Chemical Reaction)
************Simulation Time & Steps******************
20, 20           !NtotTimeSteps,NtotSnapShots
0                !ITimeStt(=0, first time run; >0, to restart based on ITimeStt-1 step)
************Initial Uniform Concentrations******************
30.3865, 0.7, 0.7         !C(particle/nm^3)///MUST Follow the above order of involved chemical components
************Boundary Condition************
!---repeat below !NthC,Ramp1Jump2,2(Flux0_End,SpringCoef_End,C_Eqilibrium_End)
0, 1, 0, 1.d3, -0.2, 0, 1.d3, 0 !electric (Displacement=Displacement0+Coef*(V-V0)) with displacement_unit:e/nm^2
1, 2, 0, 0, 0, 0, 1.d3, 30.3865 !chemical (flux=flux0+Coef*(C-C0)) with flux_unit:particle/nm^2/ns, and C_unit:particle/nm^3
2, 2, 0, 0, 0, 0, 1.d3, 0.7      !chemical (flux=flux0+Coef*(C-C0)) with flux_unit:particle/nm^2/ns, and C_unit:particle/nm^3
3, 2, 0, 0, 0, 0, 1.d3, 0.7      !chemical (flux=flux0+Coef*(C-C0)) with flux_unit:particle/nm^2/ns, and C_unit:particle/nm^3
************Numerical Parameters******************
90000, 1.d-3, 1000, 0.002        !IteratMax,ErrAllow,IteratDisplay,ARelax
**********************************************************
************All Chemical Components******************
3        !Total # of chemical components
--repeat (above #) below--!ID;Valance;Relative_Permittivity@Linear;StokesRadius;PhysicalRadius;EtaOverEpsil0((V/nm)^2-ns);AvdW0
 1,  0,   79, 0.09687,   0.1552,  0.113d1, 0.20294       !H2o(0)(10)
 2,  1,   5.55, 0.125,   0.133,   0.113d1, 0.20294       !K(1+)(39)
 3, -1,   64.4,  0.0431,   0.153,  0.113d1, 0.20294       !OH(1-)(17)
```

References

1. Dante A. B. Izzo. Michael Tong, Gang Wu, Edward P. Furlani, Numerical Analysis of Electric Double Layer Capacitors with Mesoporous Electrodes: Effects of Electrode and Electrolyte*, J. Phys. Chem. C The Journal of Physical Chemistry C, 119(45), 25235-25242. doi:10.1021/acs.jpcc.5b08409*

2. Adrian Schneuwly, Roland Gallay, Properties and Applications from state-of-the art to future trends*, 29th Annual International Computer Software and Applications Conference (COMPSAC'05). doi:10.1109/compsac.2005.95*

3. Marin S. Halper, James C. Ellenbogen, Supercapacitors: A Brief Overview

4. Martin Winter, Ralph J. Brodd, What are Batteries, Fuel Cells, and Supercapacitors?

5. Hainan Wang, Laurent Pilon, Accurate Simulations of Electric Double Layer Capacitance of Ultramicroelectrodes, *J. Phys. Chem. C The Journal of Physical Chemistry C, 115(33), 16711-16719. doi:10.1021/jp204498e*

6. Kaliyappan Karthikeyan, Samuthirapandiyan Amaresh, Sol Nip Lee, Xueliang Sun, Vanchiappan Aravindan, Young-Gi Lee, Yun Sung Lee, Construction of High-Energy-Density Supercapacitors from Pine-Cone-

Derived High-Surface-Area Carbons, *ChemSusChem, 7(5), 1435-1442.*
doi:10.1002/cssc.201301262

7.   Joseph Kestin, H. Ezzat Khalifa, Robert J. Correia, Tables of the Dynamic and Kinematic Viscosity of Aqueous NaCl Solutions in the Temperature Range 20-150°C and the Pressure Range 0.1-35 MPa.

8.   Martin Z. Bazant, Mustafa Sabri Kilic, Brian D. Storey, Armand Ajdari, Towards an understanding of induced-charged electrokinetics at large applied voltages in concentrated solutions*, Advances in Colloid and Interface Science, 152(1-2), 48-88. doi:10.1016/j.cis.2009.10.001*

9.   Concentrative Properties of Aqueous Solutions: Density, Refractive Index, Freezing Point Depression and Viscosity

10. Markus Flury, Thomas F. Gimmi, Solute Diffusion

11. Double layer (surface science). (n.d.). Retrieved May 01, 2016, from https://en.wikipedia.org/wiki/Double_layer_(surface_science)

12. A. Brandt, S. Pohlmann, A. Varzi, A. Balducci, S. Passerini, Ionic liquids in Supercapacitor

13. Wahl Sterling 2/ Sterling 6 Rechargeable Battery. (n.d.). Retrieved May 01, 2016, from http://www.wahlstore.co.uk/wahl-sterling-2-sterling-6-rechargeable-battery.ir

14. NiMH rechargeable battery 9V-Block E 200mAh maxE 1 pc. (n.d.). Retrieved May 01, 2016, from

http://www.ansmann.de/en/products/rechargeable-primary-batteries/recharcheable-batteries/e-200

15.   Capacitors for Amplifiers. (n.d.). Retrieved May 01, 2016, from http://www.mojotone.com/amp-parts/Capacitors

16.   How Capacitors Work. (n.d.). Retrieved May 01, 2016, from http://news.softpedia.com/news/How-Capacitors-Work-82563.shtml

17.   SAMWHA DH5U308W60138TH supercapacitor. (n.d.). Retrieved May 01, 2016, from http://www.tme.eu/en/pages/Product_of_the_week:samwha-dh5u308w60138th-supercapacitor.html

18.   Physical interpretation of Cyclic Voltammetry from EDLCs. (n.d.). Retrieved May 01, 2016, from https://www.seas.ucla.edu/~pilon/CV.htm

19.   File:Capacitor schematic with dielectric.svg. (n.d.). Retrieved May 01, 2016, from https://commons.wikimedia.org/wiki/File:Capacitor_schematic_with_dielectric.svg

20.   Melcher, J. R. *Continuum electromechanics*. Vol. 2 (MIT press Cambridge, 1981).

21.   Carnahan, N. F. & Starling, K. E. Equation of state for nonattracting rigid spheres. *The Journal of chemical physics* **51**, 635-636 (1969).

22. Carnahan, N. F. & Starling, K. E. Intermolecular repulsions and the equation of state for fluids. *AIChE Journal* **18**, 1184-1189 (1972).

23. Heinz, H., Vaia, R., Farmer, B. & Naik, R. Accurate simulation of surfaces and interfaces of face-centered cubic metals using $12-6$ and $9-6$ Lennard-Jones potentials. *The Journal of Physical Chemistry C* **112**, 17281-17290 (2008).

24. Wei, Y. S. & Sadus, R. J. Equations of state for the calculation of fluid-phase equilibria. *AIChE Journal* **46**, 169-196 (2000).

25. Differential Capacitance of the electric double layer: The interplay between ion finite size and dielectric decrement

26. Agency for Natural Resources and Energy, Japan

27. Qiang Gao, Optimizing carbon/carbon supercapacitors in aqueous and organic electrolytes

Biographical Information

Pranav Milind Phadtare completed his undergraduate degree in Mechanical Engineering from the University of Pune, India in May 2012. After working with Mercedes-Benz Research and Development India and Penta Designers Pvt. Ltd. As a Design Engineer, he started working towards thesis under the guidance of Dr. Bo Yang for Master's degree.

His research interests include Computer Aided Engineering, Mechanical Engineering Design, and Energy Storage Devices.